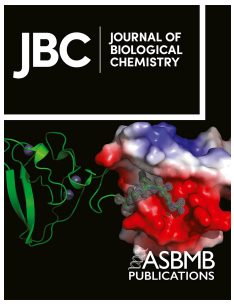

Accelerated Export of Dicer1 from Lipid-Challenged Hepatocytes Buffers Cellular miRNA-122 Levels and Prevents Cell Death

Diptankar Bandyopadhyay, Sudarshana Basu, Ishita Mukherjee, Saikat Chakrabarti, Partha Chakrabarti, Kamalika Mukherjee, Suvendra N. Bhattacharyya

PII: S0021-9258(23)02027-6

DOI: https://doi.org/10.1016/j.jbc.2023.104999

Reference: JBC 104999

To appear in: *Journal of Biological Chemistry*

Received Date: 3 January 2023

Revised Date: 19 June 2023

Accepted Date: 20 June 2023

Please cite this article as: Bandyopadhyay D, Basu S, Mukherjee I, Chakrabarti S, Chakrabarti P, Mukherjee K, Bhattacharyya SN, Accelerated Export of Dicer1 from Lipid-Challenged Hepatocytes Buffers Cellular miRNA-122 Levels and Prevents Cell Death, *Journal of Biological Chemistry* (2023), doi: https://doi.org/10.1016/j.jbc.2023.104999.

Title

Accelerated Export of Dicer1 from Lipid-Challenged Hepatocytes Buffers Cellular miRNA-122 Levels and Prevents Cell Death

Short title

Dicer1 export prevents hepatic cell death

Authors

Diptankar Bandyopadhyay[¶1], Sudarshana Basu[¶1,4],Ishita Mukherjee[2],Saikat Chakrabarti[2], Partha Chakrabarti[3], Kamalika Mukherjee[1,5] and Suvendra N. Bhattacharyya[*,1,5]

[1]RNA Biology Research Laboratory, Molecular Genetics Division, CSIR-Indian Institute of Chemical Biology, Kolkata, India

[2]Structural Biology and Bio-informatics division, CSIR-Indian Institute of Chemical Biology, Kolkata, India

[3]Metabolic Disease Laboratory, Cell Biology and Physiology Division, CSIR-Indian Institute of Chemical Biology, Kolkata, India

[4] Department of Molecular Biology, Netaji Subhas Chandra Bose Cancer Research Institute (NCRI) Kolkata, India

[5] Department of Pharmacology and Experimental Neuroscience, University of Nebraska Medical Center (UNMC), NE, USA

* Corresponding author

Tel: +1(402) 559-7558; Email: suvendra@iicb.res.in or sbhattacharyya@unmc.edu

¶ These authors contributed equally to this work

Abstract

Hepatocytes on exposure to high levels of lipids reorganize the metabolic program while fighting against the toxicity associated with elevated cellular lipids. The mechanism of this metabolic reorientation and stress management in lipid-challenged hepatocytes has not been well explored. We have noted the lowering of miR-122, a liver-specific miRNA, in the liver of mice fed with either a high-fat diet or a methionine choline-deficient diet that is associated with increased fat accumulation in mice liver. Interestingly, low miR-122 levels are attributed to the enhanced extracellular export of miRNA processor enzyme Dicer1 in mouse hepatocytes in the presence of high lipids. Export of Dicer1 can also account for the increased cellular levels of pre-miR-122- the substrate of Dicer1. Interestingly, restoration of Dicer1 levels in the mouse liver resulted in a strong inflammatory response and cell death in the presence of high lipids. Increasing death of hepatocytes was found to be caused by increased miR-122 levels in hepatocytes restored for Dicer1. Thus, the Dicer1 export by hepatocytes seems to be a key mechanism to combat lipotoxic stress by shunting out miR-122 from stressed hepatocytes. Finally, as part of this stress management, we determined that the Ago2-interacting pool of Dicer1, responsible for mature miRNP formation in mammalian cells, gets depleted. miRNA-binder and exporter protein HuR is found to accelerate Ago2-Dicer1 uncoupling to ensure export of Dicer1 via extracellular vesicles in lipid loaded hepatocytes.

Key words: miRNA; Dicer1; Extracellular Vesicles; Cell death; Lipotoxic stress

Introduction

miRNAs are 20-22 nt long non-coding regulatory RNAs that fine-tune gene expression by binding to the 3'-UTR of target mRNAs and cause their translation repression or degradation (1). miRNA biogenesis is a tightly regulated process both at the transcriptional and post-transcriptional levels and disruption of this regulation leads to various human pathologies (2-4). Dicer1, a Ribonuclease III (RNase III), processes pre-miRNA and loads the mature miRNA onto Ago2 to form the functional miRNA induced silencing complex (miRISC) in the cytoplasm of human cells (5). Dicer1 is known to be targeted for controlling cellular miRNA content (6). Majority of mammalian metabolic genes are under miRNA regulation (2) and miRNAs are known to control diverse processes in hepatic lipid metabolism including *de novo* lipogenesis, fatty acid uptake, fatty acid oxidation and triglyceride export (7). miR-122, identified as a highly abundant liver-specific miRNA accounting for almost 70% of hepatic miRNA pool is known to play a significant role in controlling hepatic metabolic processes (8, 9). Inhibition of miR-122 leads to down-regulation of several lipogenic and cholesterol biosynthesis genes in the liver (10).

Extracellular miRNAs were found to be present in body fluids including serum and saliva as freely circulating miRNAs or packaged inside vesicles (11). Extracellular vesicles (EVs) are cell derived membrane-bound vesicles that harbour an array of cargoes comprising of lipids, proteins, and nucleic acids. EVs can exert autocrine and paracrine effect by mediating intercellular communication via dynamic exchange of factors between cells and thus, helps in attaining tissue level homeostasis (12). Depending on the origin and size, EVs are broadly classified as microvesicles (which are shaded off from the plasma membrane) and exosomes (which originate from the endosomal maturation and subsequent fusion of multivesicular bodies [MVBs] with the plasma membrane) (13). Recent studies have highlighted the significance of the maturation of MVBs in modulating the activity, recycling, degradation and export of miRNPs and associated factors in animal cells (14-16). In fact, sorting and export of miRNAs into EVs are under tight regulation and governed by factors such as the RNA binding

proteins HuR and GW182 (17, 18). Thus, EV-mediated export of miRNAs can act as a means of buffering cellular miRNA pool in response to varying cellular states.

High cellular cholesterol levels coupled with endoplasmic reticulum (ER) stress has been identified as a major cause behind the pathogenesis of various metabolic disorders (19). ER-stress-dependent dysregulation of lipid metabolism may lead to dyslipidemia, insulin resistance, cardiovascular disease, type 2 diabetes, and obesity (20). It has been reported that the loading of cholesterol in macrophages induces the Unfolded Protein Response (UPR) due to the depletion of ER calcium stores (21). In response to lipid challenge, cells generally upregulate lipid droplet biogenesis to sequester excess free lipids and thus, protects the cells from lipotoxicity and associated oxidative and ER stress (22).

As lipid metabolism is known to be tightly regulated by miRNAs, lipid accumulation could, in reverse, influence miRNA biogenesis and function. But the possible mechanistic link remains underexplored. In this study, we have addressed the question of how lipid challenged hepatic cells alleviate stress due to high lipid accumulation by altering miRNA function or abundance. Short-term or long-term exposure of hepatocytes to lipotoxic stress also alters miRNA target gene network. We found, that lipid exposed hepatocytes buffer the cellular level and activity of miR-122 by exporting out the miRNA processor protein Dicer1,and thereby balances the metabolic processes. Differential compartmentalization of Dicer1 causes Dicer1-Ago2 interaction loss and subsequent export of Ago2-uncoupled Dicer1 from lipid exposed hepatocytes. The miRNA binding protein HuR, by inhibiting the interaction of miRNAs with Ago2, prevents Ago2-Dicer1 interaction to cause accelerated Dicer1 export from lipid exposed hepatocytes via EVs. This process requires maturation of endosomes and influenced by the protein Alix responsible for late endosome maturation. Dicer1 export ensures retarded *de novo* miRNP formation in hepatic cells exposed to high lipid. Similarly, MCD diet fed mice also showed decreased miR-122 and Dicer1 in liver together with increased extracellular miR-122 level detected in blood serum. Dicer1 export and associated miR-122 activity retardation in lipid exposed hepatic cells is found to be essential to prevent stress and cell death and

restoration of Dicer1 in liver of MCD diet fed mice causes increased hepatic and circulatory miR-122 levels together with elevated inflammatory cytokine production associated with death of hepatocytes expressing excess Dicer1 and experiencing lipotoxic stress.

Results

Lipotoxic stress leads to changes in miR-122 target gene network in hepatocytes

High fat exposure is known to be associated with cellular stress (23, 24). miR-122 is the key miRNA in liver to control stress response in hepatocytes(17). Is the miR-122 activity change in lipid exposed cells related to stress response? and is it inked with changed lipid metabolism in hepatic tissue? To get an overview regarding the changes in the miR-122 target gene expression in hepatic tissues under conditions of high fat exposure, differential gene expression analysis in the liver of mouse fed with high fat diet for 4 weeks, 12 weeks or high cholesterol diet for 16 weeks was performed. Short-term or long-term exposure of animals to high fat content resulted in up-regulation of 347, 2550, 184 and down-regulation of 143, 368, 38 genes in the mouse liver due to high fat diet treatment for 4 weeks (HFD4), 12 weeks (HFD12) or high cholesterol (CH) exposure for 16 weeks, respectively. A higher number of genes were found to be commonly up-regulated compared to down-regulated genes (Figure 1A and Supplementary Figure S1 and S2). Genes found to be differentially expressed in hepatocytes upon high fat exposure were analysed for probable miR-122 target sites (25). We observed that 29.37% (178 genes) of the up-regulated miR-122 target genes (total 606 genes) show a significant change in their expression levels under high fat diet treatment conditions. Moreover, among the 256 genes up-regulated in at least two or more high fat diet or cholesterol treatment conditions, 18.36% (47 genes) of them were found to be miR-122 targets (Figure 1A and Supplementary Figure S1). Numbers of lipid metabolism related genes (7 genes) were also found to be differentially regulated that are also co-regulated by miR-122 (Supplementary Figure S1). Additionally, we studied the cumulative frequency distribution of

differentially expressed genes and the predicted miR-122 target genes in hepatic tissues that had been under lipotoxic stress for 4 weeks, 12 weeks and 16 weeks (effect of cholesterol). The analysis indicates that miR-122 target mRNAs are specifically up-regulated with lipotoxic stress (Figure 1B). Pathway mapping of genes commonly up-regulated or down-regulated in high fat conditions yielded additional insights into the possible de-regulated pathways that could be associated with high fat diet regime. Such de-regulated pathways are related to carbohydrate metabolism, cellular processes and signalling pathways (Supplementary Figure S1 and S2).

Drop in cellular miR-122 content in lipid exposed hepatic cells

As there has been a substantial change in the expression of miR-122 target genes in high lipid containing hepatocytes, we wanted to follow the changes in the liver miR-122 level in mice exposed to either high fat diet or a methionine-choline deficient (MCD) diet which induce NAFLD/NASH in rodents. MCD diet causes impairment of mitochondrial β-oxidation and defective VLDL synthesis together with oxidative stress, fat accumulation in liver, liver inflammation and fibrosis (26). We noted a decrease in miR-122 level in mouse either fed with high fat diet or with methionine-choline deficient (MCD) diet (Figure 1 C, D, right panel and Supplementary Figure S3A, B). Change in miR-122 levels was associated with altered expression of lipid metabolism related genes that are known to be controlled by miR-122 (Figure 1D, left panel).

To explore the effect of cholesterol on hepatic miRNA content, we treated hepatic Huh7 cells with varying concentrations of cholesterol-lipid concentrate for 4h. Exogenous cholesterol is known to be taken up via receptor-mediated endocytosis or by bulk flow endocytosis (27) and stored as cholesteryl esters in globular structures called lipid droplets in liver cells. Quantitative estimation revealed decreased levels of miR-122 in Huh7 cells with the increase in cholesterol-lipid concentration used for treatment (Figure 1E). A similar reduction in cellular miR-122 level

was documented with increasing time of cholesterol treatment in Huh7 cells (Figure 1F). The lowering of cellular miR-122 levels upon cholesterol treatment was accompanied by an enrichment of cellular levels of its target mRNAs (namely, CAT-1 and Aldolase A) upon increasing time of exposure to cholesterol-lipid concentrate (Figure 1G). All miRNAs tested, except miR-33 and miR-16, showed a similar trend of reduced cellular levels against increasing cholesterol concentration (Figure 1H). Free fatty acid treatment (treatment with BSA conjugated Palmitic acid) also decreased mature miR-122 level in Huh7 cells in a dose-dependent manner (Figure 1I). Treatment of mouse primary hepatocytes with cholesterol or palmitate also decreased the mature miR-122 level (Figure 1J and K). Other miRNAs also showed a decrease in their cellular content upon cholesterol treatment of primary hepatocytes (Figure 1J).

Reduced level of cellular Dicer1 explains the lowering of mature miR-122 level in hepatic cells exposed to high fat

Surprisingly, upon lipid treatment, the decrease in miR-122 or other miRNAs such as miR-21 or miR-24 were not accompanied by a corresponding decrease in their precursor level rather there was an accumulation of precursor levels of these miRNAs (pre-miRNAs) upon exposure to exogenous cholesterol (Figure 2A). Palmitate treatment also led to an increase in the pre-miR-122 levels in Huh7 cells (Figure 2B). This may be indicative of decreased processing of the pre-miR-122; thereby leading to a ‘piling up’ of the same in lipid exposed cells.

We hypothesized that the accumulation of pre-miR-122 upon cholesterol treatment had something to do with the cellular level of Dicer1, a RNase III endonuclease responsible for cleaving pre-miRNA into mature miRNA. Intracellular level of Dicer1 in cholesterol treated Huh7 cells showed a gradual decrease with increase in the time of exposure to cholesterol (Figure 2C). Both, concentration, and time dependent decrease in cellular Dicer1 level on exposure to palmitate was also noted (Figure 2D-E). Similar decrease in Dicer1 level was

documented in primary hepatocytes exposed to increasing concentration of cholesterol or palmitate (Figure 2F-G). We sought to examine the effect of elevated dietary lipids on liver Dicer1 level in a high fat diet (HFD)-induced fatty liver mouse model. High fat diet fed mice liver exhibited reduced levels of Dicer1 (Supplementary Figure S3C). Liver lysates from MCD diet fed and normal chow diet (control) fed mice were analysed by western blot to detect levels of Dicer1. Similar to what was observed in high fat diet mice liver, a depleted level of Dicer1 was observed in the liver of MCD diet mice as compared to that of control diet fed mice (Figure 2H).

Extracellular vesicle mediated export from lipid challenged hepatocytes lowers cellular Dicer1 level

The lowering of Dicer1 in lipid-laden hepatocytes could either be due to reduced formation of Dicer1 protein (i.e., reduced transcription of Dicer1 mRNA) or increased degradation of Dicer1 protein. We found no significant change in Dicer1 mRNA levels upon treatment of cholesterol to Huh7 cells (Figure 2I), thus suggesting that the transcription of Dicer1 mRNA may not be affected by cholesterol treatment. To explore whether increased degradation of Dicer1 protein is responsible for its lowering in lipid treated hepatocytes, we performed experiments by inhibiting the protein degradation pathways, namely proteasomal degradation and autophagy by using specific chemical inhibitors. Inhibition of proteasome (using MG132) could not rescue the reduced cellular levels of Dicer1 in cholesterol treated Huh7 cells (Figure 2J). Similarly, inhibition of autophagy (by Bafilomycin) could not reverse the lowering of cellular Dicer1 levels upon cholesterol treatment of Huh7 cells (Figure 2K). Nevertheless, extracellular export of Dicer1 could be another effective way of reducing its cellular content. Interestingly, treatment of cells with GW4869, the inhibitor of SMNaseII, the enzyme necessary for extracellular vesicle (EV) formation (28, 29) prevented cholesterol dependent lowering of cellular Dicer1 (Figure 3A).To ascertain further that the loss of cellular Dicer1 was due to its extracellular export, we measured the levels of Dicer1 in EVs isolated from culture supernatants of Huh7 cells grown

in the presence or absence of lipids. We used HA-tagged Dicer1 (NH-Dicer1) transiently expressed in Huh7 cells to follow the export process. Cholesterol treatment decreased the levels of NH-Dicer1 in Huh7 cells (Figure 3B). EVs isolated from culture supernatants of control and lipid treated Huh7 cells were subjected to Nanoparticle Tracking Analysis (NTA) for characterization of the isolated EVs. The size versus concentration profile of the isolated EVs as obtained from NTA showed a single distinct peak at the size range of EVs (Figure 3C and D). Interestingly, treatment of cholesterol or palmitate led to an increase in the EV exocytosis (Figure 3E). However, there was a significant reduction in the mean size of EVs released from cholesterol or palmitate treated Huh7 cells as compared to that of control Huh7 cells (Figure 3F). Western blot analysis of EV extracts revealed higher amount of NH-Dicer1 in EVs isolated from cholesterol treated Huh7 cells as opposed to EVs from control Huh7 cells (Figure 3G). We also noted increase in EV-associated NH-Dicer1 in Huh7 cells exposed to palmitate for 16h (Figure 3H). Interestingly, exposure of Huh7 cells to cholesterol or palmitate led to increased extracellular export of miR-122 with a concomitant increase in miR-122 content in EVs isolated from culture supernatants of palmitate or cholesterol treated Huh7 cells (Figure 3I). RNase protection assay was done for isolated EVs to score the effect of RNase A on EV associated miR-122. We found that the EV associated miR-122 were resistant to RNase A treatment and, become sensitive to RNase A in presence of the detergent Triton X-100 (Figure 3J). This data is consistent with other reports suggesting presence of miRNAs in the lumen of EVs and thus EV-associated miRNAs are mostly resistant to RNase treatment (17, 30). The serum miR-122 level of mice exposed to MCD diet also suggests export of liver miR-122 from hepatocytes exposed to high lipid (Figure 3K). Increase in serum miR-122 levels upon MCD diet feeding could be contributed in part by hepatocyte death mediated release of miR-122 into circulation. Generally, lipotoxic stress induced hepatocyte death is largely mediated by apoptosis. Serum cytochrome c serves as a well-established marker for in vivo apoptosis (31). However, we could not detect cytochrome c in serum of MCD diet fed mice (Supplementary Figure S4A) which is indicative of negligible contribution of miR-122 released

by dead hepatocytes in the elevated serum miR-122 level in MCD diet-fed mice. To further confirm that the increase in serum miR-122 in MCD diet fed mice was contributed primarily by enhanced EV-associated miR-122, we isolated EVs from mice serum by ultracentrifugation (Supplementary Figure S4B). RT-qPCR analysis revealed a significant increase in EV associated miR-122 in MCD diet fed mice serum (Supplementary Figure S4C).

To verify the fact that the excess lipid load induces Dicer1 export from hepatocytes, we performed experiments in presence of Atorvastatin, a known chemical inhibitor of HMGCR- the enzyme that catalyses the rate-limiting step of cholesterol biosynthesis. Atorvastatin treatment is thus linked to reduced intracellular cholesterol level. Concentration dependent treatment of Huh7 cells with Atorvastatin in serum free medium enhanced the accumulation of cellular Dicer1 (Figure 3L). Consistent with this data, there was a lowering of NH-Dicer1 in EVs isolated from culture supernatants of Atorvastatin treated Huh7 cell (Figure 3M). Overall, our results support increased extracellular export of Dicer1, associated with decreased cellular levels of the protein which in turn should be linked with reduced cellular miR-122 content in lipid challenged hepatocytes.

Dicer1 export is dependent on the endosomal protein Alix

The endosomal maturation pathway gives rise to the biogenesis of multivesicular bodies (MVBs) which subsequently fuse with the plasma membrane to release EVs in the extracellular milieu. To understand the key molecular players involved in the EV packaging and export of Dicer1 and miR-122, proteins involved in the maturation of endosomes were depleted by transfecting Huh7 cells with specific siRNAs against Rab5A, Rab7A, HRS or Alix. Rab5A localizes to early endosomes where it is involved in the recruitment of Rab7A and early endosome maturation to late endosomes (32). Rab7A has been localized to late endosomes and functions as a key regulator in endo-lysosomal trafficking. It governs early-to-late endosomal maturation and endosome-lysosome transport through different protein-protein

interaction cascades (33). HRS is involved in the endosomal sorting of membrane proteins into multivesicular bodies and lysosomes. HRS mediates the initial recruitment of ESCRT-I to endosomes and, thereby, indirectly regulates multivesicular body formation (34-37). Alix, together with the lipid microenvironment, has been proposed to play a role in the formation of vesicles within multivesicular endosomes (38). Alix in association with lysobisphosphatidic acid recruits ESCRT-III proteins to the endosomes and assists in sorting and packaging of tetraspanins and other cargo proteins inside EVs (39).

Depletion of Rab5A and HRS inhibits the decrease of Dicer1 observed in siControl transfected cholesterol treated Huh7 cells (Figure 4A-B). However, there appeared to be a decrease in overall Dicer1 levels in Rab5A depleted cells even in the absence of cholesterol (Figure 4A). HRS depleted cells showed an increase in Dicer1 levels even in untreated cells (Figure 4B). Decrease of Dicer1 upon cholesterol treatment appears to be Rab7A independent (Figure 4C). Depletion of Alix by siRNA however was able to reverse the decrease in Dicer1 observed in siControl transfected cells upon cholesterol treatment (Figure 4D and E, right panel). This reversal in Dicer1 levels was accompanied by a similar reversal in cellular miR-122 levels (Figure 4E, left panel). These results led us to conclude that Alix depletion can inhibit the extracellular export of Dicer1 and miR-122 from lipid treated cells. To verify this, we isolated EVs from culture supernatants of Alix depleted Huh7 cells either treated or not treated with cholesterol-lipid concentrate. Levels of exported NH-Dicer1 and miR-122 were then analysed by western blot and RT-qPCR, respectively. Huh7 cells depleted of Alix secreted reduced levels of EV associated NH-Dicer1 and miR-122, upon cholesterol treatment (Figure 4F). NTA data of isolated EVs suggest that knockdown of Alix does not alter the size distribution or number of EVs released from untreated and cholesterol treated Huh7 cells compared to siControl transfected Huh7 cells that were untreated or treated with cholesterol, respectively (Figure 4G, 4H and S5A-D). Probably, depletion of Alix alters the sorting of Dicer1 and miR-122 into EVs leading to their reduced EV mediated export from siAlix transfected, cholesterol

treated Huh7 cells. We detected levels of various other miRNAs to see if their exocytosis was also dependent on Alix. EVs isolated from culture supernatants of siAlix transfected, cholesterol treated cells showed reduced levels of secreted miR-16, 21 and 24 with respect to siControl transfected, cholesterol treated cells (Figure 4I).

Loss of Ago2-Dicer1 interaction is coupled to enhanced Dicer1 export and reduced processing and impaired loading of mature miR-122 to Ago2 in lipid loaded Huh7 cells

In a way to reduce the activity of miR-122, hepatic cells export out cellular Dicer1 to reduce cellular burden of this stress responsive miRNA. In the process, mature miRNP levels drop and pre-miRNA levels increase. The key role of Dicer1, being an endoribonuclease, is to process the precursor miRNA duplex and load the mature miRNA strand onto Ago2 to form functional miRNP complex (40). Interaction of Dicer1 and Ago proteins has been studied extensively and has been found to be essential for miRNP formation (41-43). Surprisingly, we found that there was a substantial decrease in interaction between NH-Dicer1 and Ago2 in cholesterol-lipid treated and BSA-Palmitate treated Huh7 cells compared to the untreated Huh7 cells (Figure 5A and B). However, interaction of Ago2 with another partner protein , i.e., the P-body component Xrn1 largely remained unaltered upon lipid exposure (Figure 5C, left panel). We immunoprecipitated FH-Ago2 from control and cholesterol-lipid treated Huh7 cells and documented a reduction in the amount of miR-122 bound to FH-Ago2 in cholesterol-lipid treated Huh7 cells (Figure 5C, right panel). Thus, decreased miR-122 miRNP formation may be attributed to decreased loading of miR-122 from Dicer1 to Ago2 due to the reduced interaction of these two proteins in high lipid condition. Does loss of Ago2-Dicer1 interaction have a role in Dicer1 processing of pre-miR-122? In earlier experiments, we have observed an accumulation of pre-miR-122 in lipid treated Huh7 cells (Figure 2A, left panel and 2B). To delineate the mechanism, we immunoprecipitated NH-Dicer1 from cholesterol-lipid treated and control Huh7 cells and noticed an increase of miR-122 and miR-122* association with NH-Dicer1 from cholesterol-lipid treated Huh7 cells (Figure 5D). This was accompanied by a

reduction of pre-miR-122 association with NH-Dicer1 in cholesterol-lipid treated Huh7 cells (Figure 5E). However, cholesterol treatment does not completely impede the nuclear to cytosolic translocation of pre-miR-122 as we noted accumulation of pre-miR-122 in both the nuclear and cytosolic fractions of cholesterol treated Huh7 cells (Supplementary Figure S6). Since, Dicer1 is not able to load the mature miR-122 onto Ago2, probably due to reduced Ago2-Dicer1 interaction, so the already processed miR-122 along with the miR-122* remains bound to Dicer1. As a result, Dicer1 does not become available for the next round of processing of a new pre-miR-122 molecule. The decrease in Dicer1-bound pre-miR-122 could be either due to differential subcellular localization of cytoplasmic pre-miR-122 and Dicer1 or inability of Dicer1 to bind a fresh pre-miR-122 molecule as its active site might remain blocked by miR-122 and miR-122* strands which could not be loaded onto Ago2 possibly due to differential cellular distribution of the proteins Ago2 and Dicer1. Interestingly, there was no change in interaction between NH-Dicer1 and Ago2 in Alix depleted cholesterol treated Huh7 cells compared to siControl transfected cholesterol exposed Huh7 cells (Figure 5F). Therefore, the Dicer1-Ago2 interaction loss must happen upstream of EV packaging and export of Dicer1-miR-122 complex.

Spatial redistribution of ER and endosomes is associated with loss of interaction of Ago2 and Dicer1 in lipid loaded Huh7 cells

Exploring the mechanistic link between high lipid exposure and export of Dicer1 in hepatic cells, we did subcellular fractionation to check the cellular Dicer1 distribution in mammalian hepatic cells before and after lipid treatment. Surface of the rough endoplasmic reticulum (rER) has been reported as the site of miRNP nucleation and *de novo* miRNP formation (43, 44). rER also serves as the site where mRNAs interact with the repressive miRNPs before they are trafficked to endosomal compartment for subsequent degradation (16). Huh7 cells were used to prepare microsome which are enriched for rER proteins. Microsomes have been identified as the sites for miRNA-mediated repression of target mRNAs and also the site for

miRNP biogenesis (16, 45). We analysed the association of Dicer1 with microsomal fractions isolated from Huh7 cells grown in presence and absence of high lipids and documented specific loss of Dicer1 from microsomal fraction in lipid-treated cells whereas no major change in Ago2 association with microsome was noted (Supplementary Figure S7A-B).

To decipher the cause of Ago2 uncoupling from Dicer1, isotonic lysates of Huh7 cells transiently expressing NH-Dicer1 were fractionated on a 3-30% iodixanol (Opti-prep™) density gradient to separate out individual organelles as shown in Figure 5G. From western blot analysis of the subcellular fractions shown in Figure 5H, an enrichment of NH-Dicer1 in the endosomal/MVB fractions (marked by enrichment of the MVB marker protein Alix) together with a decrease of the same from the ER fractions (marked by enrichment of the ER marker protein Calnexin) was observed. Thus, cholesterol treatment caused a change in the compartmentalisation of NH-Dicer1 from the ER to endosomal/MVB fractions and that may be the reason of Ago2-Dicer1 interaction loss. This endosomal/MVB enrichment of NH-Dicer1 might be either due to an active translocation of NH-Dicer1 from the ER to the endosomes/MVBs or by retarded retrograde recycling of NH-Dicer1 from MVBs to the ER compartment that has also been described in the context of mitochondrial depolarization (43).

To confirm the enhanced endosomal association of Dicer1, Huh7 cell lysates (transiently expressing NH-Dicer1) were further fractionated on a 3-15% iodixanol (Opti-prep ™) density gradient (Supplementary Figure S7C). The aim was to separate the early endosomal fractions from the late endosomes and to determine the differential association of NH-Dicer1 with these fractions in presence of cholesterol. Fractions 2-4 were enriched for early endosomes (EE) (based on colocalization with the marker protein Alix), and fractions 6-9 represented late endosomes (LE) positive for the marker Rab7A (Supplementary Figure S7C). We observed Dicer1 association with both fractions in the absence of cholesterol. However, in cholesterol loaded cells NH-Dicer1 was found to be predominantly lost from fractions 6 and 7 that are heavier than the EE positive fractions (Supplementary Figure S7C).

RT-qPCR analysis of miR-122 in the ER and endosome/MVB fractions of control versus cholesterol treated Huh7 cells showed a decrease of miR-122 from the ER upon cholesterol treatment (Figure 5I), suggesting a lowered level of active pool of miR-122 specific miRNPs which generally remains enriched at the ER. But, endosome/MVB associated miR-122 showed no appreciable change upon cholesterol treatment which indirectly hints at the endosome/MVB enrichment of miR-122 while total cellular miR-122 decreases upon cholesterol treatment (Fig 1E and F). Subcellular distribution of miR-122* revealed a significant enrichment at the endosome/MVB fractions with no significant change at the ER fractions upon cholesterol treatment (Supplementary Figure S8A). However, unlike miR-122 which was found to get elevated in EVs isolated from the culture supernatants of cholesterol treated Huh7 cells, we could not detect miR-122* in EVs isolated from culture supernatants of control or cholesterol treated Huh7 cells (Supplementary Figure S8B). This was accompanied by elevated levels of miR-122* in cholesterol treated Huh7 cells (Supplementary Figure S8C). Although, both miR-122 and miR-122* get enrichment at the endosome/MVBs, miR-122 gets selectively packaged into EVs whereas miR-122* accumulates inside cells.

Interestingly, upon immuno-precipitation of NH-Dicer1 from the endosomal/MVB fractions, we found a reduction in association of miR-122 with NH-Dicer1 upon cholesterol treatment (Figure 5J). This was accompanied by a reduction in NH-Dicer1 associated Ago2 in the MVB fractions of cholesterol treated Huh7 cells (Figure 5K). Probably, MVB associated NH-Dicer1 cannot interact with Ago2 and thus, releases the bound miR-122 at the MVBs for packaging and release as part of EVs. In the process, NH-Dicer1 also remains associated with MVBs and thus, itself gets exocytosed as well.

Lastly, we performed microscopic analysis to visualize the spatial distribution of Endoplasmic Reticulum and endosomal compartments in lipid loaded cells by expressing an ER localizing variant of DsRed (ER-DsRed) and endosome localizing variant of GFP (Endo-GFP) in Huh7 cells. Cholesterol treated cells appeared to show a more peripheral endosomal distribution

(green) with respect to control non-treated cells. In control cells, endosomes appeared as discrete organelles (green) associated with the ER (red) and homogenously distributed throughout the cytoplasm. However, in cholesterol treated cells they appeared either as large perinuclear bodies or aligned with the periphery of the cell. There were also reduced association of endosomes with the ER in treated cells (Figure 5L). The surface reconstructed 3D images of ER and endosomes created from z-stack images clearly showed a redistribution of endosomes towards the cell periphery together with a decrease in ER-endosomal contact sites in cholesterol loaded cells (Figure 5L). This intrigues us to hypothesize that probably, the altered distribution and rearrangement of ER-endosomal contacts upon lipid loading influences the loss of Ago2-Dicer1 interaction thus, hindering the retrograde transport of NH-Dicer1 from endosomes to ER known to be required for *de novo* formation of miRNPs (43).

Elevated level of HuR mediates exocytosis of Dicer1 from lipid loaded Huh7 cells

The human ELAV protein HuR is a well-known stress response factor that translocate to the cytoplasm to facilitate relief of repressed mRNAs in response to starvation (46). It also binds miRNAs with specificity and has been reported to bind and ensure export of miR-122 and let-7a from hepatic Huh7 and non-hepatic HeLa cells (17). HuR is also known to relocalize to the cytoplasm in lipid challenged cells (47). Does HuR play a role to facilitate Dicer1 export? There was a loss of Ago2 association of miR-122 in Huh7 cells treated with cholesterol (Figure 5C, right panel). We noted elevated cellular levels of HuR in Huh7 cells treated with cholesterol-lipid concentrate in a dose dependent manner (Figure 6A). To find out whether HuR has any role in modulating the abundance of Dicer1 in lipid treated cells, we performed experiments in HuR depleted Huh7 cells. Interestingly, depletion of HuR could inhibit the cellular decrease in Dicer1 levels in cholesterol-lipid treated Huh7 cells (Figure 6B). Interestingly, ectopic expression of HA-HuR in Huh7 cells led to a decrease in cellular Dicer1 levels (Figure 6C). Previous reports suggest the importance of HuR in packaging and export of miR-122 from amino acid starved Huh7 cells (17). To this end, we investigated the role of HA-HuR in export

of Dicer1 from Huh7 cells. Surprisingly, ectopic expression of HA-HuR led to elevated levels of NH-Dicer1 in EVs compared to its content in EVs from pCIneoco-transfected Huh7 cells (Figure 6D). Interestingly, HA-HuR expression also led to a reduction in Ago2-Dicer1 interaction (Figure 6E). HuR has three RNA binding domains (RRM I, II and III) and a spacer region between RRMII and III. Deletion mutants without one of the RRMs or the spacer hinge region (ΔB) were analysed for their effect of Dicer1 export. It seems except the RRMΔIII variant all the other variants of HuR are capable of lowering Dicer1 in Huh7 cells (Figure 6F-G). Ectopic expression of Ago2 in the form of FH-Ago2 could restore Dicer1 level in cholesterol treated cells (Figure 6H). However, HA-HuR mediated Dicer1 lowering could not be restored by ectopic expression of FH-Ago2 (Figure 6I). HuR is known to uncouple miRNA from Ago2 but does not show any interaction with Ago2 in immunoprecipitation reaction (17). The RRMIII of HuR is reported to be important for its role in miRNA binding and export (17) and now found to be important for Dicer1 export also. Therefore, HuR possibly work on Ago2-miRNA complex to uncouple miRNA from Ago2 and lower the Dicer1-Ago2 interaction possibly by favouring a differential compartmentalization of miRNA uncoupled Ago2 and Dicer1 in mammalian cells. The effect of HuR is substantial and enhanced cellular Ago2 levels that otherwise can restore cellular Dicer1 level in lipid-exposed cells, fails to do so in cells ectopically expressing HuR.

Lowering of Dicer1 and subsequent reduced level of miR-122 acts as a cellular survival mechanism to counter the growing ER stress levels in lipid exposed hepatic cells

Our results demonstrate that increase in cellular lipid content leads to the export of Dicer1 from hepatocytes. But the possible role of this efflux and its physiological significance remained unknown. To answer this question, we expressed NH-Dicer1 in cholesterol-lipid treated Huh7 cells to enhance the Dicer1 level and had estimated the mRNA levels of genes that have shown upregulated expression in high lipid conditions in the bioinformatic analysis (Figure 7A). We found further elevations in levels of LDLR, HMGCR, ACAT2 and SCD in NH-Dicer1 expressing lipid treated cells (Figure 7B). This could have been possible only if the loss

of Dicer1 was a pre-requisite to combat cellular stress via downregulation of miR-122 biogenesis in lipid loaded cells. By overexpressing Dicer1, the stress condition might have been further increased as signified by elevated levels of lipid metabolic genes that were upregulated in lipid challenged hepatic cells possibly due to miR-122 restoration upon ectopic expression of NH-Dicer1.

Excess lipid exposure of Huh7 in the form of cholesterol or fatty acids caused elevated levels of lipid droplets as observed by Bodipy493/503 staining and subsequent microscopy analysis (Fig 7C). We further wanted to determine if lipid exposure of Huh7 cells leads to increased ER stress. To test that, we detected levels of phosphorylated eIF2α in cholesterol treated Huh7 cells. We observed increased phosphorylation of eIF2α along with elevated levels of cleaved PARP (Figure 7D). Palmitate treatment also induces ER stress (Figure 7E). Therefore, lipid treatment appeared to lead to an increase in ER stress levels and apoptosis as observed in the western blot data of Phospho-eIF2α and cleaved PARP in Huh7 cells (Figure 7D and E). The accumulation of lipid droplets in lipid loaded Huh7 cells plays a protective role to prevent lipotoxic stress arising from excess free lipid accumulation and associated oxidative stress and ER stress. In fact, induction of ER stress to Huh7 cells by treatment with the ER stress inducer, Thapsigargin, was accompanied by a reduction in cellular Dicer1 levels in a dose dependent manner (Fig 7F). It also led to an accumulation of LDs as evident in the microscopic images (Fig 7G). These data reinforce the hypothesis of cellular Dicer1 reduction is a way of stress relief for hepatic cells. ER stress induction was verified by elevated levels of phospho-eIF2α upon Thapsigargin treatment (Fig 7F). Earlier studies demonstrated that Thapsigargin caused an increase in EV mediated export of miR-122 in Huh7 cells to relieve stress (17). Thus, there might be a possible link between lipid-induced ER stress and EV-mediated miR-122 and Dicer1 secretion. Effect of expression of NH-Dicer1 on augmented stress response was confirmed in detection of elevated levels of Phospho-eIF2α and cleaved PARP in NH-Dicer1 transfected cholesterol treated Huh7 cells compared to cholesterol treated control

Huh7 cells not expressing NH-Dicer1 (Figure 7H). TUNEL staining revealed increased number of TUNEL positive nuclei in NH-Dicer1 expressing cells treated with cholesterol-lipid concentrate for 4 and 8 hours (Figure 7I and J). Cells transfected with NH-Dicer1 expression plasmids showed an increased percentage of TUNEL positive nuclei with respect to non-transfected cells upon lipid treatment (Figure 7J). Thus, extracellular secretion of Dicer1 possibly acts as a survival mechanism adopted to counteract the growing lipotoxicity within the hepatic cell.

To investigate whether elevated miR-122 levels in NH-Dicer1 expressing Huh7 cells exposed to cholesterol was responsible for increased stress and apoptosis, we measured the levels of phospho-eIF2α and cleaved PARP levels after inhibition of miR-122 by anti-miR-122 oligos. Interestingly, we detected reduced cleaved PARP level in NH-Dicer1 expressing, cholesterol treated Huh7 cells that were transfected with anti miR-122. However, miR-122 inactivation had no major effect on phospho-eIF2α (Figure 7K). Therefore, the effect of increased miR-122 on apoptosis may work in a phospho-eIF2α independent or downstream pathway.

Restoration of Dicer1 in MCD-diet fed mice liver increases stress and expression of pro-inflammatory cytokines

We wanted to check the importance of Dicer1 and miR-122 loss in lipid exposed hepatocyte to conclude on their role in metabolic regulation in the liver of mice experiencing the lipotoxic stress. The mice were fed either a normal chow diet (control diet) or MCD diet, and a group of MCD-diet fed mice were injected with NH-Dicer1 expression plasmid through tail-vein to restore the Dicer1 in the liver (Figure 8A). Compared to control diet fed or MCD diet fed group of mice, the mice on MCD diet but expressing NH-Dicer1 showed a substantial increase in mature miR-122 level (Figure 8B, left panel). However, another miRNA, i.e., miR-21 level did not show an increase in NH-Dicer1 expressing, MCD diet fed mice liver (Figure 8B, right panel), thus suggesting that restoration of Dicer1 in liver of mice may have a more pronounced effect on miR-122 the most abundant miRNA in liver. The increased level of pre-miR-122

observed in MCD diet fed group was restored to control level upon NH-Dicer1 expression (Figure 8B, middle panel). The miRNA-122 target CAT-1 mRNA expression also dropped below control level upon NH-Dicer1 expression in MCD-diet fed mice (Figure 8C, left panel). Interestingly, the mature serum miR-122 level that has already been increased in MCD diet fed group increased further in the serum of mice fed with MCD diet and expressing NH-Dicer1 (Figure 8C, right panel). This was accompanied by an increase in phospho-eIF2α and decreased phospho-eIF4EBP1 levels in MCD diet fed group of animals expressing NH-Dicer1 in the liver (Figure 8D). These data signify an increased stress in MCD diet fed mice liver that get enhanced further with restored Dicer1 which results in elevated miR-122 level in mice liver. Expression of HuR also increases with MCD diet that restored to normal level upon NH-Dicer1 expression. These data were further corroborated with the observation of higher amount of fat deposition in the MCD diet fed mice liver expressing NH-Dicer1 (Figure 8E-G). The increased fat deposition noted in the histological section was associated with increased level of pro-inflammatory cytokine IL-1β and TNF-α mRNAs as detected in the MCD diet fed mice liver expressing NH-Dicer1 (Figure 8H).

Discussion

Our findings have highlighted a unique mechanism adapted by hepatocytes to alleviate stress due to excess lipid load by lowering cellular miR-122 levels. Hepatocytes do so by actively exporting out miR-122 and the pre-miRNA processor protein Dicer1. Bioinformatic analysis revealed that miR-122 target genes which participate in the metabolic processes (ACSS2, ACACB) were down-regulated upon short term high fat exposure. However, miR-122 target genes (44) like CTNNB1, PDGFRA, PDGFRB, CCND1 or PRKCB involved in regulating cellular process or signalling pathways become up-regulated only upon prolonged exposure to high fat content.

Modulation of Dicer1 availability, stability and abundance or tight regulation of Dicer1 activity is employed in cells to balance the mature miRNA expression. TAR RNA binding protein (TRBP) and protein kinase R-activating protein (PACT) are known to interact with Dicer1 and causes stabilization and enhanced processivity of Dicer1 (42, 48). Various signalling pathways are also known to modulate the abundance and activity of Dicer1. Phosphorylation of TRBP2 by MAPK/ERK pathway is known to stabilize Dicer1 and increase Dicer1 activity leading to the expression of growth-promoting miRNAs and reduction of let-7a which is a tumour suppressor miRNA (49). Variation in the 5'-UTR of Dicer1 mRNA and their restricted expression pattern in a tissue specific manner suggests another layer of regulation (50). The pluripotency factor Lin-28 is also known to inhibit processing of pre-let 7 RNA by Dicer1 in embryonic stem cells and embryocarcinoma cells (51). In another report it has been shown how a protozoan parasite specific protease reduces hepatic cell Dicer1 to inhibit biogenesis of miR-122 and thereby, stop cholesterol production in liver cell. This is important for sustained infection by the pathogen where restoration of Dicer1 in infected liver can clear the infection (6). The present study reports EV mediated extracellular export of Dicer1 and miR-122 as a novel way of buffering cellular miRNA levels in lipid loaded Huh7 cells. While miRNAs are known to regulate lipid metabolic processes, our findings suggest the existence of a reciprocal mechanism of controlling miRNA levels in lipid exposed hepatic cells.

Non-alcoholic steatohepatitis is accompanied by altered expression profile of miRNAs in liver (52). Thus, in order to understand the role of miRNAs in the pathophysiology of NASH, it is necessary to understand the mechanisms that govern the altered expression of hepatic miRNAs during NASH progression. Lowering of Dicer1 levels in lipid-laden hepatocytes is expected to have an impact on the global miRNA profile of hepatocytes via downregulation of pre-miRNA processing. Accordingly, we find reduction of several miRNAs, namely, miR-122, miR-24 and miR-21 in cholesterol treated Huh7 cells. The lowering of these miRNAs might act as an adaptation to increased lipid load and could have a protective role against lipotoxic stress since, studies have shown that the inhibition of these miRNAs are associated with

reduced hepatic lipid accumulation and partial amelioration of NASH in mice (10, 53, 54). Surprisingly, we find increased levels of miR-33 and miR-16 upon cholesterol treatment to Huh7 cells. This could be attributed to the existence of other regulatory mechanisms that contribute to the modulation of these miRNAs. For example, miR-33 is transcribed from the intronic region of the sterol-regulatory element-binding protein (SREBP) transcription factor and functions in tandem with SREBPs to attain cholesterol and lipid homeostasis (55). Nevertheless, the selective accumulation of these miRNAs in lipid treated Huh7 cells could be due to the upregulation of transcription of these pri-miRNAs, increased half-life/stability of the mature miRNAs, selective storage of theses miRNAs in compartments such as the P-bodies, reduced extracellular export or preferential processing of their precursor forms under limiting Dicer1 levels. Exploration of such possibilities could give us useful insights about the re-organization of the miRNA profile in lipid loaded hepatocytes.

Marked loss of Ago2-Dicer1 interaction in lipid treated Huh7 cells, causes impaired assembly of miRNA loading complex. Since, miRNA biogenesis is coupled to RISC activity, loss of Ago2-Dicer1 interaction causes reduced loading of miR-122 to Ago2 rendering reduced functional miR-122 specific miRNP formation. Concomitantly, Dicer1 processivity decreases as its active site remains associated with the mature miRNA strands (miR-122 and miR-122*) and hence, it cannot bind a new pre-miR-122 molecule for processing. This is evident from increased association of NH-Dicer1 with miR-122 and miR-122*, together with reduced association of NH-Dicer1 with pre-miR-122 in lipid loaded Huh7 cells.

Cholesterol treatment was found to cause an enrichment of miR-122 and miR-122* at the endosome/MVB. However, selective packaging of the sense strand, i.e., miR-122 into the endosome/MVB facilitated its EV mediated release into the extracellular milieu, whereas the antisense strand, i.e, miR-122* failed to get packaged and exported as part of EVs. As a result, miR-122* got accumulated in cholesterol treated Huh7 cells. Studies have shown the selective or simultaneous enrichment of the sense and antisense strand of a particular miRNA could

occur in a tissue specific or developmental stage specific manner that can target completely different sets of mRNAs to regulate the cellular transcriptome (56, 57). Accordingly, the miRNA arm switching from miR-122 to miR-122* in lipid loaded Huh7 cells could act to modulate the transcriptome in a way to cope up with the growing lipotoxicity.

Stability and processivity of Dicer1 is known to be governed by its interaction with other factors (42, 48). Thus, observed translocation of Dicer1 from ER to MVBs upon lipid treatment could be attributed to its reduced interaction with Ago2 which might lead to alteration in its stability, post-translational modifications or interaction with other factors that ultimately aid in MVB packaging of Dicer1. This mechanism may be universal as loss of Dicer1 from non-hepatic cells has also been observed under lipid exposure (Supplementary Figure S9A). We have found how Dicer1-Ago2 interaction loss caused by ectopic expression of HuR can enhance the export of Dicer1 to allow lowering of miRNA activity in cells experiencing lipotoxic stress (Figure 9). Interestingly, upon NH-Dicer1 expression in mouse liver followed by MCD diet has reduced the expression of HuR that otherwise get enhanced in the liver of mice fed with MCD diet. This data suggests Dicer1 may negatively regulate HuR expression possibly by upregulating some HuR targeting miRNAs. Lowered HuR level can also account for the increased cellular level of miR-122 in mice liver cells expressing NH-Dicer1 and fed with MCD diet.

The exported miR-122 is involved in activation of resident macrophage in lipid exposed liver that elevate the pro-inflammatory pathways in recipient cells (58). We have noted EV-mediated export of Dicer1 also from lipid exposed liver cells that may also contribute to processing of pre-miRNA associated with EVs even in recipient cells. The implications of EV-associated Dicer1 in the context of epigenetic signal transmission across the tissue of cells is not clear. However, it is clear from the data presented here that dual export of mature miR-122 and Dicer1 from hepatic cells is a useful mechanism for the hepatocytes to balance the miRNA activity. The effect on miR-122 is more prominent as miR-122 is the most abundant

and active miRNA in liver that regulate majority of the metabolic and cell growth pathways in liver cells (9). Thus, modulation of the mature miR-122 levels through regulation of Dicer1 is a useful mechanism for hepatocyte to combat lipid induced stress. The effect of lipids on miRNAs that showed unaltered or increase abundance in lipid exposed hepatocytes may be coupled with increased transcription of pri-miRNA or preferential stabilization/processing of those miRNAs under limiting Dicer1 levels in lipid exposed cells.

The miR-122 released by hepatocytes have the capacity to induce expression of inflammatory cytokines when delivered to macrophages as evident from previous reports (58). It is interesting to note that enhanced serum level of miR-122 in MCD diet fed mice expressing NH-Dicer1 in the liver signifies the importance of this regulation and elevated circulatory miR-122 level may be associated with high inflammatory status across tissues where the liver specific miR-122 may elicit a strong inflammatory response by activating resident macrophages. The chronic changes in gene expression in non-hepatic tissues in NAFLD may thus be attributed by high circulatory miRNAs derived from liver.

Experimental Procedures

Cell culture and transfections

Huh7 cells were cultured in Dulbecco's Modified Eagle's Medium (DMEM) supplemented with 2mM L-glutamine and 10% heat inactivated fetal calf serum (Gibco) and 1% Penicillin-Streptomycin.

All plasmid transfections to Huh7 cells were done with Lipofectamine 2000 (Invitrogen), according to the manufacturer's protocol. 1µg of plasmid was transfected per well of a six-well plate. siRNAs were transfected using RNAiMAX (Invitrogen), according to the manufacturer's protocol. 30 picomoles of respective siRNAs were transfected per well of a twelve-well plate. Transfections were done overnight (16 hours) followed by splitting of cells to a larger growing surface area.

Cholesterol and Palmitic Acid treatment

MβCD conjugated cholesterol obtained from Gibco (#12531-018) was added from a 250X stock to Huh7 cells or primary hepatocytes in culture at a final concentration of 1X, 2X or 5X for a period of 2, 4 or 8 hours (30mg/L effective cholesterol in 1X). Cholesterol treatments were done to Huh7 cells or primary hepatocytes in fresh growth media at 70-80% confluency. Unless otherwise mentioned, cholesterol treatment was done at a final concentration of 5X (150 mg/l) for 4 hours.

Palmitic acid (Sigma) was conjugated to fatty acid free BSA (Sigma) in KRBH buffer (NaCl 135mM, KCl 3.6mM, $NaHCO_3$ 5mM, NaH_2PO_4 0.5mM, HEPES 10mM, $MgCl_2$ 0.5mM, $CaCl_2$ 1.5mM, D-glucose 3.5 mM, BSA 21%) at 37^0C for 6 hours in a shaking condition. Final concentration of this working stock is 10mM with a BSA:Palmitic Acid ratio of 1:3. The BSA conjugated Palmitic acid was then filter sterilized and added to Huh7cells or primary hepatocytes at a final concentration of 100, 300, 500 or 1000µM for 16 hours. For control (0 µM), equal amount of fatty acid free BSA in KRBH buffer was added. All treatments were done to Huh7 cells or primary hepatocytes in fresh growth media at 50-60% confluency.

Statin Treatment

For inhibition of HMG-CoA reductase, Huh7 cells were cultured in serum free Dulbecco's modified Eagle's medium (DMEM; Gibco-BRL) for 24 h at 60% confluency. Atorvastatin stock concentration of 1mg/ml (1.78 mM) was prepared in UltraPure distilled water and added to the cells cultured in serum free DMEM at concentrations of 0, 1, 5 and 10 µM. Cells were subsequently incubated over a time period of 48 hours.

Western Blot

Cell lysates or immunoprecipitated protein extracts were subject to SDS-polyacrylamide gel electrophoresis followed by transfer of proteins to a polyvinylidene difluoride (PVDF) membrane (Milipore). The membranes were blocked for 1 hour in blocking buffer (containing

Tris-buffered saline (TBS), 0.1% Tween20 and 3% BSA) at room temperature. The blots were then incubated with primary antibodies in blocking buffer for a minimum time of 16 hours at 4^0C. This was followed by washing of the blots thrice for 5 min each in TBS containing 0.1% Tween 20. The blots were then probed with HRP-conjugated secondary antibodies in blocking buffer (1:8000 dilution) for 1 hour at room temperature. Excess antibodies and non-specific bindings were washed off with TBS-Tween 20 thrice for 5 min each. Developing and imaging of all the western blots signals was done in UVP Bioimager 600 system equipped with VisionWorks Life Science software (UVP) V6.80 using either SuperSignal™ West Femto, Luminata Forte Western HRP Substrate or SuperSignal™ West Pico Maximum Sensitivity Substrate. Quantification of band intensitieswas done using ImageJ software. Unless otherwise mentioned, normalization of band intensities of specific proteins was done with respect to β-actin band intensity of the same lane.

RNA isolation and quantification of miRNA and mRNA levels

RNA isolation was done using TRIzol reagent (Life Technologies) according to the manufacturer's protocol. Real-time quantitative RT-PCR of mRNA was done with 100-200ng of RNA by a two-step reaction format using Eurogentec Reverse Transcriptase Core Kit and MESA GREEN qPCR Master Mix Plus for SYBR Assay-Low ROX. 18S ribosomal RNA was used as an endogenous control. For expression of lipid metabolic genes, β-Actin mRNA was used as an endogenous control.

Real-time quantitative RT-PCR of miRNAs, namely miR-122, miR-16, miR-21, miR-24, miR-33, miR-29awere done with 25ng of total isolated RNA using Applied Biosystems TaqMan chemistry-based assays, following the manufacturer's instructions. U6 snRNA was used as the endogenous control. For detection of miRNAs in extracellular vesicle fractions, 100ng of isolated RNA was used for reverse transcription in each case.

All PCR reactions were done in either 7500 Applied Biosystem Real Time System or BIO-RAD CFX96 Real-Time system. The Reverse Transcription reaction conditions were 16^0C for 30 min, 42^0 C for 30 min, 85^0C for 5 min, followed by product held at 4^0C. The PCR conditions were 95^0C for 5 min, followed by 40 cycles of 95^0C for 15 seconds, 60^0C for 1 min.

Extracellular Vesicles (EV) isolation

For all EV related experiments cells were grown in media supplemented with EV depleted FCS. EV depleted FCS was either commercially obtained (System Biosciences Catalog no. EXO-FBS-250A-1) or prepared by ultracentrifugation of the FCS at 120,000 x g for 5 hours. For EV isolation, the supernatant conditioned media (CM) from two 60 cm^2 plates, having $6x10^6$ donor cells (Huh7) each were taken. CM were pre-cleared by centrifugation at 300 x g for 10min, 2,000 x g for 15 min, 10,000 x g for 30 min at 4^0 C and subsequently, filtered through a 0.22 µm filter unit. The resultant filtrate was then loaded on top of a sucrose cushion (1 M sucrose and 10 mM Tris–HCl pH 7.5) and ultracentrifugation was done at 1,00,000 x g for 90 min at 4^0 C. The media above the sucrose cushion was then discarded till the interface leaving behind a narrow layer of medium where the EVs get enriched. The EVs where then washed with PBS by ultracentrifugation at 100,000xg for 90 min at 4^0 C. The pellet was resuspended in 200 µl 1X Passive Lysis Buffer (Promega) and divided into two parts for protein and RNA analysis, respectively. For Nanoparticle Tracking Analysis (NTA), the EV pellets were resuspended in 200 µl PBS followed byfurther dilution of the EV samples in PBS was done. 1 ml of the diluted EV samples were injected into the sample channel of the Nanoparticle Tracking Analyzer (NanoSight NS300) for subsequent analysis.

RNase protection assay of EV associated miR-122

To identify whether EV associated miR-122 are present on the EV surface or inside EV lumen, an RNase protection assay of EVs was employed. Initially, EVs were isolated from conditioned media of cholesterol treated Huh7 cells (12×10^6) by a two-step ultracentrifugation method as

earlier described. Isolated EVs were resuspended in ice-cold PBS followed by digestion with RNase A (100µg/ml) at 30^0C for 60 mins in presence or absence of Triton X-100. Post reaction, RNase inactivation and residual RNA extraction was done using Trizol LS reagent following manufacturer's protocol and qRT-PCR detection of miR-122 was done.

Subcellular fractionation on OptiPrep™ density gradients

Cell fractionation was done on a OptiPrep™density gradient as previously described (59). Briefly, a 3-30% or 3-15.5% OptiPrep™ (Sigma) continuous gradient was prepared in a buffer containing 78 mM KCl, 4 mM $MgCl_2$, 10 mM EGTA, 50 mM HEPES pH 7.0. Cells were harvested and washed in ice-cold PBS followed by homogenization using a Dounce homogenizer in a buffer containing 0.25 M sucrose, 78 mM KCl, 4 mM $MgCl_2$, 8.4 mM $CaCl_2$, 10 mM EGTA, 50 mM HEPES pH 7.0 along with 100 µg/ml Cycloheximide, 0.5 mM DTT, 40 U/ml RNase Inhibitor (Applied Biosystems), 1X Protease inhibitor (Roche). The lysate was cleared by centrifugation at 1,000g for 5 min, twice. The clarified lysate was loaded on top of the OptiPrep™density gradient and ultracentrifuged at 133,000xg for 5h using Beckman Coulter SW60Ti rotor at 4^0 C. After ultracentrifugation, ten fractions were collected by aspiration from top of the tubes. The fractions were then processed for RNA or protein analysis.

Microsome isolation

Microsomes were isolated from Huh7 cells as previously described (45). Briefly, Huh7 cells were washed with PBS and resuspended in 1X hypotonic buffer (containing 10 mM HEPES, pH 7.8, 1 mM EGTA, 25 mM KCl) proportionate to three times packed cell volume for 20 min on ice. The cells were then resuspended in 1X isotonic buffer (10 mM HEPES, pH 7.8, 1 mM EGTA, 25 mM KCl, 250mM sucrose) proportionate to two times packed cell volume, followed by homogenization. The homogenate was clarified by centrifugation at 1,000xg for 5 min. The supernatant was centrifuged at 12,000xg for 10 mins in order to remove the mitochondrial

fraction. The post-mitochondrial supernatant was incubated with 8M $CaCl_2$ for 30 min at 4^0 C in a rotator, followed by centrifugation at 8,000xg for 10 min to get the microsomal pellet.

Nuclear and cytosolic fractionation

Untreated and cholesterol treated Huh7 cells were initially washed with PBS, re-suspended in cytosolic extraction buffer [containing 10 mM HEPES pH 7.9, 10 mM KCl, 0.1 mM EDTA, 0.1% NP-40, 1X Protease inhibitor (Roche), 40 U/ml RNase Inhibitor (Applied Biosystems)] proportionate to five times of the packed cell volume and incubated on ice for 10 minutes with mild vortexing from time to time. The resultant solution was then centrifuged at 800 xg for 5 min at 4^0C followed by collection of the supernatant which is the crude cytosolic extract. The pellet obtained was washed thrice in cytosolic extraction buffer (without NP-40) by centrifugation at 800 xg for 5 min at 4^0C to remove cytosolic contaminants. Subsequently, the pellet was re-suspended in equal volume of nuclear extraction buffer [containing 20 mM HEPES pH 7.9, 0.4 M NaCl, 1 mM EDTA, 25% Glycerol, 1X Protease inhibitor (Roche), 40 U/ml RNase Inhibitor (Applied Biosystems)] and incubated on ice for 20 min with mild vortexing from time to time. Finally, the solution was centrifuged at 17,000 xg for 5 min at 4^0C and the supernatant containing the nuclear extract was harvested. The crude cytosolic extract obtained earlier was further centrifuged at 17,000 xg for 5 min at 4^0C to get the supernatant as the final cytosolic extract. The nuclear and cytosolic extracts were then further processed for RNA and protein analysis. RNA was isolated from the nuclear and cytosolic extracts using Trizol LS reagent followed by RT-qPCR analysis of pre-miR-122 was done. For protein analysis, the extracts were subjected to SDS-PAGE followed by western blot analysis of the nuclear and cytosolic marker proteins.

Immunoprecipitation

Immunoprecipitation of indicated proteins was carried out according to the published method (46). Briefly, cells were lysed in a lysis buffer [containing 20mM Tris-HCl pH 7.4, 150mM KCl,

5mM $MgCl_2$, 1 mM dithiothreitol (DTT), 1X EDTA-free protease inhibitor (Roche), 40 U/ml RNase Inhibitor (Applied Biosystems), 0.5% Triton X-100, 0.5% sodium deoxycholate] for 30 min at 4^0 C. The lysate was cleared by centrifugation at 3,000xg for 10 min. Protein G Agarose beads (Invitrogen) were blocked with 5% BSA in lysis buffer for 1h. The beads were then allowed to bind to the required antibody for 3-4 h at 4^0C in lysis buffer, followed by addition of the lysate. A final dilution of 1:100 (anibody:lysate) was used for immunoprecipitation. All immunoprecipitations were done for 16 h at 4^0C followed by bead washing thrice in IP Buffer [containing 20mM Tris-HCl pH 7.4, 150mM KCl, 5mM $MgCl_2$, 1 mM dithiothreitol (DTT), 1X EDTA-free protease inhibitor (Roche), 40U/ml RNase Inhibitor (Applied Biosystems)]. The beads were then divided into two parts; one part for RNA isolation and the other part for western blot analysis.

TUNEL Assay

TUNEL assay was performed using Invitrogen Click-iT™ TUNEL Alexa Fluor 594 Imaging Assay kit for HA-DICER1 expressing Huh7 cells, as per manufacturer's protocol.

Immunofluorescence Microscopy and post-imaging analysis

Cells grown on gelatin coated 18 mm round coverslips were transfected and treated as indicated. Cells were then fixed with 4% para-formaldehyde in PBS for 30 min at room temperature in dark. For immunostaining, blocking and permeabilization was done in 1% BSA in PBS containing 0.1% Triton X-100 and 10% goat serum (Gibco) for 30 min at room temperature followed by probing with appropriate primary antibodies for 16h at 4^0C. The coverslips were washed thrice in PBS followed by staining for 1h at room temperature with Alexa Fluor® anti-rabbit, anti-mouse or anti-rat secondary IgG conjugated to appropriate fluorochrome (Molecular probes). For lipid droplet staining, cells grown on gelatin coated coverslips were probed with Bodipy 493/503 (Invitrogen) diluted in PBS at a final concentration of 5 µM for 30 mins at room temperature. Coverslips were finally mounted on cleaned glass

slides using VECTASHIELD mounting medium (with DAPI). Confocal fixed-cell imaging was done with Zeiss LSM 800 confocal system. All post imaging analysis was done using Imaris 7 (BitPlane) software.

Animal experiments

All animal experiments were approved by the Institutional Animal Ethics Committee (approved by CPCSEA, Ministry of Environment & Forest, and Government of India). 8-10 weeks old male C57BL/6 mice weighing (20-24g) were housed under controlled conditions (temperature 23 ± 2℃, 12 hour/12-hour light/dark cycle) in individually ventilated cages. Mice were randomly divided into two groups and fed either standard chow diet or Methionine Choline deficient diet MCD (MP Biomedicals; #0296043910) for up to four weeks.

C57BL/6 male mice of 8-10 weeks age were divided in two groups for normal chow and high fat diet (HFD) containing 45% fat and 5.81 kcal/gm diet energy content (MP Biomedicals; # 960192). Animals were fed with HFD for 4 weeks.

For expression of NH-Dicer1 in mouse liver,8-10 weeks old male C57BL/6 mice were randomly divided into three groups and housed in individually ventilated cages at a temperature of 23 ± 2°Cand 12-hour light/ 12-hour dark cycle with free access to food and water. Control group was fed with normal chow diet for 4 weeks. The other two groups were fed a Methionine Choline deficient (MCD) [MP Biomedicals; #0296043910] diet for 4 weeks accompanied by tail vein injection of 30 µg plasmid/mouse with either NH-Dicer1 expression plasmid or control plasmid (pCIneo). Tail vein injections were administered on the 10th, 18th and 24th day of the feeding period. Endotoxin free plasmids were isolated from transformed bacterial cells using Sure Prep Plasmid Endofree Maxi kit (cat no. #NP-15363). On the 4th day following the last dose of tail vein injection, blood samples were collected by cardiac puncture and then mice were sacrificed and liver was isolated. One lobe of the liver from each mouse

was fixed in 10% neutral-buffered formalin for subsequent histological analysis. The rest of the liver tissue was snap-frozen and stored at -80^{0}C for protein and RNA analysis.

For western blot analysis, liver tissue lysates were prepared from approximately 10 mg of liver slice by homogenization in 1x RIPA buffer (containing 50 mM Tris–HCl pH 7.4, 150 mM NaCl, 1% NP-40, 0.5% sodium deoxycholate, 0.1% SDS and 1mM phenylmethylsulfonyl fluoride) followed by sonication and cleared by centrifugation at 20,000 x g for 1 hour. For liver tissue RNA preparation, liver slices of approximately 10 mg were homogenized in Trizol reagent followed by RNA isolation as per manufacturer's protocol. For serum isolation, blood samples were initially allowed to sediment at room temperature for 2 hours followed by centrifugation at 2,500 x g at 4^{0}C and subsequent collection of supernatants. Serum RNA was isolated using Trizol LS reagent as per manufacturer's protocol. Quantification of relative levels of miRNA and mRNA in liver tissue and serum were done by qRT-PCR from isolated RNA.

For histological analysis, tissues were fixed in 10% neutral-buffered formalin, embedded in paraffin, and sectioned at 5 µm thickness. Formalin fixed and paraffin embedded liver tissue sections of 5 µm thickness were deparaffinized in xylene followed by rehydration of the sections was done in graded concentrations of ethanol. The sections were then stained for hematoxylin and eosin. Images were captured using an inverted light microscope. Image analysis for quantification of fat globule number and hepatic fat globule diameter were done with ImageJ software.

Primary Hepatocyte Isolation

Animals were obtained from the animal house of the institute and all experiments were performed according to the guidelines set by Institutional Animal Ethics committee following the Govt. of India regulations. Mouse primary hepatocytes were isolated using the hepatocyte product line from Gibco Invitrogen Corporation. Adult BALB/c mice (4-6 weeks) were anaesthetized and the portal vein was cannulated using a 25G butterfly cannula and an

incision was made in the inferior vena cava. The liver was perfused with 350 mL of warm (37°C) Liver Perfusion Medium (Cat. No. 17701) at a rate of 35 mL/minute with the perfusate exiting through the severed vena cava. This was followed by a Collagenase-Dispase digestion with Liver Digest Medium (Cat no. 17703) at a rate of 35 mL/minute. The liver was then aseptically transferred to the tissue culture hood on ice in Hepatocyte Wash Medium (cat no. 17704). Using blunt forceps, the digested liver was torn open to release the hepatocytes. Cell clumps were dissociated by gently pipetting the solution up and down using a 25ml pipette. The solution was then filtered through 100 µM nylon caps atop 50 ml conical tubes. The cell suspension was then centrifuged at 50 x g for 3 min. The pellet was gently resuspended in 10 ml of Wash Medium using 25 ml pipette and the centrifugation repeated.

Cells were finally resuspended in Hepatocyte Wash Medium with 10% FCS and plated at $1x10^7$ cells /ml. Cells were plated in tissue culture treated collagen (Gibco Cat. No. A10483-01) coated plates at 12.5µg/cm^2. Unattached cells are poured off 4h after plating and medium was replaced with Hepatozyme-SFM (Cat no. 17705) with glutamine and 1% Pen/Strep. Cholesterol and BSA-Palmitate was added the next day in Hepatozyme-SFM.

Statistical Analysis

All graphs were plotted and analysed using GraphPad Prism 5.00 and 8.00 versions (GraphPad, San Diego, CA, USA). For statistical analysis, non-parametric two-tailed, paired or unpaired Student's *t*-test was performed. For more than two groups of data in Figure 1 and 2, one-way analysis of variance (one-way ANOVA) followed by Tukey's post-hoc test was performed. Error bars indicate mean with standard deviation.

Differential expression analysis and pathway mapping

In order to determine alterations in hepatic gene expression profile under lipotoxic stress and study the possible physiological relevance of expression changes in miR-122 target genes, differentially expressed genes and their pathway involvement has been studied. Differential

expression analysis was performed considering high fat diet fed mouse versus chow diet fed mouse for 4 weeks, 12 weeks and mice having high fat along with cholesterol diet as opposed to only high fat diet for 16 weeks. Samples from GSE53381 [high fat diet treatment for 4 weeks (HFD4)] and GSE93819 [high fat diet treatment for 12 weeks (HFD12)] (60) datasets were considered to identify genes that are involved in regulating short term or long term high fat diet exposure associated stress. Additionally, samples from GSE58271 (61) were considered to identify genes involved in responding to high cholesterol (CH) exposure associated stress. For this purpose, differentially expressed genes were determined with the help of limma (62) R package in Gene Expression Omnibus (GEO) series datasets (63). Genes having fold change >= 1.5 and p-value <= 0.05 were considered as differentially expressed and are likely to be involved in regulating lipotoxic species associated stress. A probable set of miR-122 target mRNA was determined based on a previous study (25) wherein livers of miR122a$^{-/-}$ mice had been compared with wild-type mice. mRNA that had fold change in expression higher than 1.5 or lower than -1.5 with significant p-values have been considered as miR-122 target mRNAs. Venn diagrams were utilised to determine miR-122 target genes that showed altered levels under two or more of these conditions. Further, we determined whether miR-122 target genes are enriched in liver cells of high fat diet fed mice under lipotoxic stress. Here, the cumulative frequency distribution of differentially expressed genes under lipotoxic stress, and the de-regulated miR-122 target genes were compared. Additionally, pathway mapping of miR-122 target genes differentially expressed in two or more of the high fat diet treatment conditions was performed. The genes were mapped onto KEGG database (64, 65) pathways with the help of a python script. Cellular pathways belonging to the categories such as ‘carbohydrate metabolism’, ‘lipid metabolism’, ‘cellular process’ and ‘signal transduction and signalling molecules and interaction’ were considered for the analysis. A plot was prepared to determine whether the high fat diet exposure associated miR-122 target genes participated in multiple signalling or metabolic pathways and as such whether alterations in miR-122 target genes may bring about time dependent physiological changes.

miR-122 target genes that exhibited high fat diet exposure associated alterations were represented in rows with their corresponding pathway involvement(s) being shown in columns and each cell depicted the conditions under which they exhibit alterations.

Information on Plasmids, Oligos, miRNA assay IDs, PCR primers, Antibodies are provided as Supporting Information Table S1-S5.

Data Availability

All data supporting the findings of this study are available from the corresponding authors upon request.

Conflict of Interest

The authors declare no conflict of interest

Acknowledgements

We thank Witold Filipowicz and Gunter Meister for different constructs used in this study. We thank the Funding body, Dept. of Science and Technology (DST), Govt. of India and Council for Scientific and Industrial Research (CSIR), and University Grant Commission (UGC) for the fellowship to DB, SB, IM, RC,KM and MA. SB also acknowledges the support from Department of Biotechnology, Govt of India for her Fellowship support. SNB is supported by The Swarnajayanti Fellowship (DST/SJF/LSA-03/2014-15) from Dept. of Science and Technology, Govt. of India. The work also received support from a High-Risk High Reward Grant (HRR/2016/000093) from Dept. of Science and Technology, Govt. of India and CEFIPRA project grant 6003-J. SNB Also acknowledge the Start-Up Support Grant of University of Nebraska, USA.

Author Contributions

S.N.B. and K.M. conceived the idea, designed the experiments and analysed the data. S.B. D.B., S.C. and P.C have contributed in design and planning the experiments. D.B., S.B., I.M., performed the experiments. S.B. and D.B also wrote the manuscript with S.N.B. and analysed the data.

References

1. Bartel, D. P. (2018) Metazoan MicroRNAs Cell **173**, 20-51 10.1016/j.cell.2018.03.006
2. Bartel, D. P. (2009) MicroRNAs: target recognition and regulatory functions Cell **136**, 215-233 10.1016/j.cell.2009.01.002
3. Filipowicz, W., Bhattacharyya, S. N., andSonenberg, N. (2008) Mechanisms of post-transcriptional regulation by microRNAs: are the answers in sight? Nature reviews Genetics **9**, 102-114 10.1038/nrg2290
4. Esquela-Kerscher, A., andSlack, F. J. (2006) Oncomirs - microRNAs with a role in cancer Nature reviews Cancer **6**, 259-269 10.1038/nrc1840
5. Kim, V. N., Han, J., andSiomi, M. C. (2009) Biogenesis of small RNAs in animals Nat Rev Mol Cell Biol **10**, 126-139 10.1038/nrm2632
6. Ghosh, J., Bose, M., Roy, S., andBhattacharyya, S. N. (2013) Leishmania donovani targets Dicer1 to downregulate miR-122, lower serum cholesterol, and facilitate murine liver infection Cell Host Microbe **13**, 277-288 10.1016/j.chom.2013.02.005
7. Liu, W., Cao, H., Yan, J., Huang, R., andYing, H. (2015) 'Micro-managers' of hepatic lipid metabolism and NAFLD Wiley interdisciplinary reviews RNA **6**, 581-593 10.1002/wrna.1295
8. Chang, J., Nicolas, E., Marks, D., Sander, C., Lerro, A., Buendia, M. A. *et al.* (2004) miR-122, a mammalian liver-specific microRNA, is processed from hcr mRNA and may downregulate the high affinity cationic amino acid transporter CAT-1 RNA biology **1**, 106-113, http://www.ncbi.nlm.nih.gov/pubmed/17179747
9. Jopling, C. (2012) Liver-specific microRNA-122: Biogenesis and function RNA biology **9**, 137-142 10.4161/rna.18827
10. Esau, C., Davis, S., Murray, S. F., Yu, X. X., Pandey, S. K., Pear, M. *et al.* (2006) miR-122 regulation of lipid metabolism revealed by in vivo antisense targeting Cell Metab **3**, 87-98 10.1016/j.cmet.2006.01.005
11. Gallo, A., Tandon, M., Alevizos, I., andIllei, G. G. (2012) The majority of microRNAs detectable in serum and saliva is concentrated in exosomes PLoS One **7**, e30679 10.1371/journal.pone.0030679
12. Stahl, P. D., andRaposo, G. (2019) Extracellular Vesicles: Exosomes and Microvesicles, Integrators of Homeostasis Physiology (Bethesda) **34**, 169-177 10.1152/physiol.00045.2018
13. van Niel, G., D'Angelo, G., andRaposo, G. (2018) Shedding light on the cell biology of extracellular vesicles Nat Rev Mol Cell Biol **19**, 213-228 10.1038/nrm.2017.125
14. Gibbings, D. J., Ciaudo, C., Erhardt, M., andVoinnet, O. (2009) Multivesicular bodies associate with components of miRNA effector complexes and modulate miRNA activity Nature cell biology **11**, 1143-1149 10.1038/ncb1929

15. Lee, Y. S., Pressman, S., Andress, A. P., Kim, K., White, J. L., Cassidy, J. J. *et al.* (2009) Silencing by small RNAs is linked to endosomal trafficking Nature cell biology **11**, 1150-1156 10.1038/ncb1930
16. Bose, M., Barman, B., Goswami, A., andBhattacharyya, S. N. (2017) Spatiotemporal Uncoupling of MicroRNA-Mediated Translational Repression and Target RNA Degradation Controls MicroRNP Recycling in Mammalian Cells Molecular and cellular biology **37**, 10.1128/MCB.00464-16
17. Mukherjee, K., Ghoshal, B., Ghosh, S., Chakrabarty, Y., Shwetha, S., Das, S. *et al.* (2016) Reversible HuR-microRNA binding controls extracellular export of miR-122 and augments stress response EMBO reports **17**, 1184-1203 10.15252/embr.201541930
18. Ghosh, S., Mukherjee, K., Chakrabarty, Y., Chatterjee, S., Ghoshal, B., andBhattacharyya, S. N. (2021) GW182 Proteins Restrict Extracellular Vesicle-Mediated Export of MicroRNAs in Mammalian Cancer Cells Molecular and cellular biology **41**, 10.1128/MCB.00483-20
19. Sozen, E., andOzer, N. K. (2017) Impact of high cholesterol and endoplasmic reticulum stress on metabolic diseases: An updated mini-review Redox Biol **12**, 456-461 10.1016/j.redox.2017.02.025
20. Basseri, S., andAustin, R. C. (2012) Endoplasmic reticulum stress and lipid metabolism: mechanisms and therapeutic potential Biochemistry research international **2012**, 841362 10.1155/2012/841362
21. Feng, B., Yao, P. M., Li, Y., Devlin, C. M., Zhang, D., Harding, H. P. *et al.* (2003) The endoplasmic reticulum is the site of cholesterol-induced cytotoxicity in macrophages Nature cell biology **5**, 781-792 10.1038/ncb1035
22. Olzmann, J. A., andCarvalho, P. (2019) Dynamics and functions of lipid droplets Nat Rev Mol Cell Biol **20**, 137-155 10.1038/s41580-018-0085-z
23. Anderson, E. K., Hill, A. A., andHasty, A. H. (2012) Stearic acid accumulation in macrophages induces toll-like receptor 4/2-independent inflammation leading to endoplasmic reticulum stress-mediated apoptosis Arteriosclerosis, thrombosis, and vascular biology **32**, 1687-1695 10.1161/ATVBAHA.112.250142
24. Fu, S., Watkins, S. M., andHotamisligil, G. S. (2012) The role of endoplasmic reticulum in hepatic lipid homeostasis and stress signaling Cell Metab **15**, 623-634 10.1016/j.cmet.2012.03.007
25. Wen, J., andFriedman, J. R. (2012) miR-122 regulates hepatic lipid metabolism and tumor suppression The Journal of clinical investigation **122**, 2773-2776 10.1172/JCI63966
26. Anstee, Q. M., andGoldin, R. D. (2006) Mouse models in non-alcoholic fatty liver disease and steatohepatitis research International journal of experimental pathology **87**, 1-16 10.1111/j.0959-9673.2006.00465.x
27. Strauss, K., Goebel, C., Runz, H., Mobius, W., Weiss, S., Feussner, I. *et al.* (2010) Exosome secretion ameliorates lysosomal storage of cholesterol in Niemann-Pick type C disease The Journal of biological chemistry **285**, 26279-26288 10.1074/jbc.M110.134775
28. Luberto, C., Hassler, D. F., Signorelli, P., Okamoto, Y., Sawai, H., Boros, E. *et al.* (2002) Inhibition of tumor necrosis factor-induced cell death in MCF7 by a novel inhibitor of neutral sphingomyelinase The Journal of biological chemistry **277**, 41128-41139 10.1074/jbc.M206747200
29. Essandoh, K., Yang, L., Wang, X., Huang, W., Qin, D., Hao, J. *et al.* (2015) Blockade of exosome generation with GW4869 dampens the sepsis-induced inflammation and cardiac dysfunction Biochimica et biophysica acta **1852**, 2362-2371 10.1016/j.bbadis.2015.08.010
30. Ghoshal, B., Bertrand, E., andBhattacharyya, S. N. (2021) Non-canonical ago loading of EV-derived exogenous single stranded miRNA in recipient cells Journal of cell science 10.1242/jcs.253914

31. Barczyk, K., Kreuter, M., Pryjma, J., Booy, E. P., Maddika, S., Ghavami, S. *et al.* (2005) Serum cytochrome c indicates in vivo apoptosis and can serve as a prognostic marker during cancer therapy Int J Cancer **116**, 167-173 10.1002/ijc.21037
32. Hunker, C. M., Galvis, A., Kruk, I., Giambini, H., Veisaga, M. L., andBarbieri, M. A. (2006) Rab5-activating protein 6, a novel endosomal protein with a role in endocytosis Biochemical and biophysical research communications **340**, 967-975 10.1016/j.bbrc.2005.12.099
33. Feng, Y., Press, B., andWandinger-Ness, A. (1995) Rab 7: an important regulator of late endocytic membrane traffic The Journal of cell biology **131**, 1435-1452, http://www.ncbi.nlm.nih.gov/pubmed/8522602
34. Colombo, M., Moita, C., van Niel, G., Kowal, J., Vigneron, J., Benaroch, P. *et al.* (2013) Analysis of ESCRT functions in exosome biogenesis, composition and secretion highlights the heterogeneity of extracellular vesicles Journal of cell science **126**, 5553-5565 10.1242/jcs.128868
35. Hurley, J. H., andHanson, P. I. (2010) Membrane budding and scission by the ESCRT machinery: it's all in the neck Nat Rev Mol Cell Biol **11**, 556-566 10.1038/nrm2937
36. Pons, V., Luyet, P. P., Morel, E., Abrami, L., van der Goot, F. G., Parton, R. G. *et al.* (2008) Hrs and SNX3 functions in sorting and membrane invagination within multivesicular bodies PLoS biology **6**, e214 10.1371/journal.pbio.0060214
37. Scoles, D. R., Huynh, D. P., Chen, M. S., Burke, S. P., Gutmann, D. H., andPulst, S. M. (2000) The neurofibromatosis 2 tumor suppressor protein interacts with hepatocyte growth factor-regulated tyrosine kinase substrate Human molecular genetics **9**, 1567-1574, http://www.ncbi.nlm.nih.gov/pubmed/10861283
38. Piper, R. C., andKatzmann, D. J. (2007) Biogenesis and function of multivesicular bodies Annual review of cell and developmental biology **23**, 519-547 10.1146/annurev.cellbio.23.090506.123319
39. Larios, J., Mercier, V., Roux, A., andGruenberg, J. (2020) ALIX- and ESCRT-III-dependent sorting of tetraspanins to exosomes The Journal of cell biology **219**, 10.1083/jcb.201904113
40. Bose, M., andBhattacharyya, S. N. (2016) Target-dependent biogenesis of cognate microRNAs in human cells Nat Commun **7**, 12200 10.1038/ncomms12200
41. Kolb, F. A., Zhang, H., Jaronczyk, K., Tahbaz, N., Hobman, T. C., andFilipowicz, W. (2005) Human dicer: purification, properties, and interaction with PAZ PIWI domain proteins Methods in enzymology **392**, 316-336 10.1016/S0076-6879(04)92019-8
42. Haase, A. D., Jaskiewicz, L., Zhang, H., Laine, S., Sack, R., Gatignol, A. *et al.* (2005) TRBP, a regulator of cellular PKR and HIV-1 virus expression, interacts with Dicer and functions in RNA silencing EMBO reports **6**, 961-967 10.1038/sj.embor.7400509
43. Bose, M., Chatterjee, S., Chakrabarty, Y., Barman, B., andBhattacharyya, S. N. (2020) Retrograde trafficking of Argonaute 2 acts as a rate-limiting step for de novo miRNP formation on endoplasmic reticulum-attached polysomes in mammalian cells Life science alliance **3**, 10.26508/lsa.201800161
44. Stalder, L., Heusermann, W., Sokol, L., Trojer, D., Wirz, J., Hean, J. *et al.* (2013) The rough endoplasmatic reticulum is a central nucleation site of siRNA-mediated RNA silencing The EMBO journal **32**, 1115-1127 10.1038/emboj.2013.52
45. Barman, B., andBhattacharyya, S. N. (2015) mRNA Targeting to Endoplasmic Reticulum Precedes Ago Protein Interaction and MicroRNA (miRNA)-mediated Translation Repression in Mammalian Cells The Journal of biological chemistry **290**, 24650-24656 10.1074/jbc.C115.661868
46. Bhattacharyya, S. N., Habermacher, R., Martine, U., Closs, E. I., andFilipowicz, W. (2006) Relief of microRNA-mediated translational repression in human cells subjected to stress Cell **125**, 1111-1124 10.1016/j.cell.2006.04.031

47. Lu, S., Mott, J. L., andHarrison-Findik, D. D. (2015) Saturated fatty acids induce post-transcriptional regulation of HAMP mRNA via AU-rich element-binding protein, human antigen R (HuR) The Journal of biological chemistry **290**, 24178-24189 10.1074/jbc.M115.648212
48. Chendrimada, T. P., Gregory, R. I., Kumaraswamy, E., Norman, J., Cooch, N., Nishikura, K. *et al.* (2005) TRBP recruits the Dicer complex to Ago2 for microRNA processing and gene silencing Nature **436**, 740-744 10.1038/nature03868
49. Paroo, Z., Ye, X., Chen, S., andLiu, Q. (2009) Phosphorylation of the human microRNA-generating complex mediates MAPK/Erk signaling Cell **139**, 112-122 10.1016/j.cell.2009.06.044
50. Singh, S., Bevan, S. C., Patil, K., Newton, D. C., andMarsden, P. A. (2005) Extensive variation in the 5'-UTR of Dicer mRNAs influences translational efficiency Biochemical and biophysical research communications **335**, 643-650 10.1016/j.bbrc.2005.07.138
51. Rybak, A., Fuchs, H., Smirnova, L., Brandt, C., Pohl, E. E., Nitsch, R. *et al.* (2008) A feedback loop comprising lin-28 and let-7 controls pre-let-7 maturation during neural stem-cell commitment Nature cell biology **10**, 987-993 10.1038/ncb1759
52. Cheung, O., Puri, P., Eicken, C., Contos, M. J., Mirshahi, F., Maher, J. W. *et al.* (2008) Nonalcoholic steatohepatitis is associated with altered hepatic MicroRNA expression Hepatology **48**, 1810-1820 10.1002/hep.22569
53. Ng, R., Wu, H., Xiao, H., Chen, X., Willenbring, H., Steer, C. J. *et al.* (2014) Inhibition of microRNA-24 expression in liver prevents hepatic lipid accumulation and hyperlipidemia Hepatology **60**, 554-564 10.1002/hep.27153
54. Rodrigues, P. M., Afonso, M. B., Simao, A. L., Carvalho, C. C., Trindade, A., Duarte, A. *et al.* (2017) miR-21 ablation and obeticholic acid ameliorate nonalcoholic steatohepatitis in mice Cell Death Dis **8**, e2748 10.1038/cddis.2017.172
55. Rottiers, V., andNaar, A. M. (2012) MicroRNAs in metabolism and metabolic disorders Nat Rev Mol Cell Biol **13**, 239-250 10.1038/nrm3313
56. Ro, S., Park, C., Young, D., Sanders, K. M., andYan, W. (2007) Tissue-dependent paired expression of miRNAs Nucleic Acids Res **35**, 5944-5953 10.1093/nar/gkm641
57. Griffiths-Jones, S., Hui, J. H., Marco, A., andRonshaugen, M. (2011) MicroRNA evolution by arm switching EMBO reports **12**, 172-177 10.1038/embor.2010.191
58. Das, A., Basu, S., Bandyopadhyay, D., Mukherjee, K., Datta, D., Chakraborty, S. *et al.* (2021) Inhibition of extracellular vesicle-associated MMP2 abrogates intercellular hepatic miR-122 transfer to liver macrophages and curtails inflammation iScience **24**, 103428 10.1016/j.isci.2021.103428
59. Chakrabarty, Y., andBhattacharyya, S. N. (2017) Leishmania donovani restricts mitochondrial dynamics to enhance miRNP stability and target RNA repression in host macrophages Molecular biology of the cell 10.1091/mbc.E16-06-0388
60. Kobori, M., Takahashi, Y., Sakurai, M., Ni, Y., Chen, G., Nagashimada, M. *et al.* (2017) Hepatic Transcriptome Profiles of Mice with Diet-Induced Nonalcoholic Steatohepatitis Treated with Astaxanthin and Vitamin E International journal of molecular sciences **18**, 10.3390/ijms18030593
61. Lorbek, G., Perse, M., Jeruc, J., Juvan, P., Gutierrez-Mariscal, F. M., Lewinska, M. *et al.* (2015) Lessons from hepatocyte-specific Cyp51 knockout mice: impaired cholesterol synthesis leads to oval cell-driven liver injury Scientific reports **5**, 8777 10.1038/srep08777
62. Ritchie, M. E., Phipson, B., Wu, D., Hu, Y., Law, C. W., Shi, W. *et al.* (2015) limma powers differential expression analyses for RNA-sequencing and microarray studies Nucleic Acids Res **43**, e47 10.1093/nar/gkv007

63. Barrett, T., Wilhite, S. E., Ledoux, P., Evangelista, C., Kim, I. F., Tomashevsky, M. *et al.* (2013) NCBI GEO: archive for functional genomics data sets--update Nucleic Acids Res **41**, D991-995 10.1093/nar/gks1193
64. Cokelaer, T., Pultz, D., Harder, L. M., Serra-Musach, J., andSaez-Rodriguez, J. (2013) BioServices: a common Python package to access biological Web Services programmatically Bioinformatics **29**, 3241-3242 10.1093/bioinformatics/btt547
65. Kanehisa, M., andGoto, S. (2000) KEGG: kyoto encyclopedia of genes and genomes Nucleic Acids Res **28**, 27-30 10.1093/nar/28.1.27

Figure Legends

Figure 1 Altered expression of miR-122 target genes in the high fat diet-fed mice liver with associated loss of miR-122 from hepatocytes

(A) Numbers of differentially expressed genes and miR-122 target genes in the liver of mice after high fat diet. Hepatocytes from mouse having fed high fat diet exhibit alterations in expression of miR-122 target genes. A comparison of genes de-regulated in various high fat diet case studies (HFD12, HFD4, CH) has been shown here. Numbers of genes and miR-122 targets that are mainly up-regulated or down-regulated upon high fat diet treatment are shown and compared against the changes observed in the liver of miR-122 knock-out mice (first two panels from left). Number of miR-122 target mRNAs associated with lipid metabolism which were found to be up-regulated (third panel from left) or down-regulated (fourth panel from left) under high fat diet treatment conditions are also shown. HFD12 – High fat diet treatment for 12 weeks, HFD4 – High fat diet treatment for 4 weeks, CH – Cholesterol treatment for 16 weeks, miR122- miR122 knockout mice.

(B) miR-122 target gene enrichment analysis. The cumulative distribution function (CDF) plot of the differentially expressed mRNA and miR-122 target genes, under high fat diet conditions are shown here. Left panel shows changes observed after high fat diet treatment for 4 weeks (HFD4), middle panel depicts changes after high fat diet treatment for 12 weeks (HFD12) and right panel shows changes after cholesterol treatment for 16 weeks (CH16).

(C, D) Levels of mRNA of lipid metabolic genes and miRNAs in the liver of normal chow diet fed and Methionine Choline Deficient (MCD) diet fed mice. Schematic representation of the experiment is shown in panel (C). 8-10 weeks old male C57BL/6 mice were fed either a normal chow diet (ND) or Methionine Choline deficient diet (MCD) for 4 weeks. Quantification of mRNAs of lipid metabolic genes in the liver of MCD diet fed mice was performed (D, left panel, n = 3 independent experiments; P = 0.0096, 0.0617, 0.0122, 0.1304, respectively). qRT-PCR based detection and quantification using gene specific primers was done from 200 ng of RNA isolated from mice liver lysates. Normalization was done using β-Actin mRNA. Lipid accumulation in the liver of Methionine Choline deficient (MCD) diet fed mice leads to reduction in miRNA levels (D, right panel, n = 3 independent experiments; P = 0.0127, 0.5528, 0.0669, 0.0543, respectively). qRT-PCR based detection of miRNAs was done from 25 ng of RNA isolated from liver lysates. Normalization was done by U6 snRNA.

(E) Scheme of the experiment (left panel). Changes in cellular levels of miR-122 upon treatment of Huh7 cells with increasing concentration of cholesterol-lipid concentrate for 4

hours (right panel). miR-122 levels were quantified by qRT-PCR based detection from 25 ng of isolated cellular RNA. Normalization was done against U6 snRNA (n = 3 independent experiments; P = 0.0009).

(F) Time dependent changes in cellular miR-122 content in cholesterol-lipid concentrate treated (150 mg/l) Huh7 cells. miR-122 levels were quantified by quantitative qRT-PCR detection from 25 ng of isolated cellular RNA. Normalization was done against U6 snRNA (n = 3 independent experiments; P = 0.0008).

(G) Changes in cellular levels of miR-122 target mRNAs CAT1 (left panel, n ≥ 3 independent experiments; P = 0.0007) and Aldolase A (right panel, n = 4 independent experiments; P < 0.0001) upon increasing time of cholesterol treatment (150 mg/l) in Huh7 cells. Levels of CAT1 and Aldolase A were detected by qRT-PCR from 200 ng of cellular RNA and normalised against GAPDH mRNA levels.

(H) Cellular levels of different miRNAs in Huh7 cells treated with cholesterol-lipid in a concentration dependent manner for 4 hours. All miRNA levels were quantified by qRT-PCR detection from 25 ng of isolated cellular RNA. Normalization was done against U6 snRNA (n = 3 independent experiments; P = 0.0009, <0.0001, 0.0001, 0.1406, 0.0385, respectively).

(I) Changes in cellular miR-122 content in Huh7 cells treated with increasing concentration of BSA conjugated palmitic acid (BSA-Palmitate) for 16 hours. For 0 mM treatment condition, equivalent amount of fatty acid free BSA was added as done in experimental group. 25 ng of isolated cellular RNA was used for qRT-PCR measurement of miR-122 levels. Normalization was done against U6 snRNA (n = 4 independent experiments; P = 0.0205).

(J) qRT-PCR based quantification of indicated miRNAs from mouse primary hepatocytes cultured *in vitro* and treated with or without cholesterol concentrate (150 mg/l) for 4 hours. Cellular miRNA contents were quantified by qRT-PCR detection from 25 ng of isolated cellular RNA. Data was normalized with respect to U6 snRNA (n = 3 independent experiments; P = 0.0449, <0.0001, 0.0593, 0.0081, respectively).

(K) Cellular miR-122 levels in mouse hepatocytes treated with either fatty acid free BSA (0 mM palmitate) or 1 mM of BSA-Palmitate for 16 hours. qRT-PCR measurement of miR-122 was done with 25 ng of isolated cellular RNA. Data normalized against U6 snRNA (n = 3 independent experiments; P = 0.0199).

Data are represented as mean ± SD; ns: non-significant, *P < 0.05, **P < 0.01, ***P < 0.001, ****P<0.0001. For more than two groups of data (E-I), P-values were calculated using a one-

way analysis of variance (one-way ANOVA) with Tukey post-hoc test. Otherwise, P-values were calculated by utilising two-tailed, Student's *t*-test.

Figure 2 Reduction in cellular Dicer1 level accounts for loss of mature miRNA in hepatocyte after exposure to high lipids

(A) Precursor miR-122 (left panel, n = 4 independent experiments; P = 0.0030), precursor miR-21 (middle panel, n ≥ 3 independent experiments; P = 0.0021) and precursor miR-24 (right panel, n ≥ 3 independent experiments; P = 0.0008) cellular levels in Huh7 cells treated with cholesterol-lipid concentrate (150 mg/l) for indicated time points. qRT-PCR detection of precursor levels was done from 200 ng of isolated cellular RNA. 18S rRNA levels were used for normalization.

(B) Changes in cellular pre-miR-122 content in Huh7 cells treated with increasing concentration of BSA conjugated palmitic acid (BSA-Palmitate) for 16 hours. For 0 mM treated Huh7 cells, equivalent amount of fatty acid free BSA was treated for 16 hours. Pre-miR-122 cellular levels were measured with 200 ng of cellular RNA by qRT-PCR and normalized against 18S rRNA levels (n = 3 independent experiments; one-way AVOVA; P = 0.0343).

(C) Western blot analysis of Dicer1 levels in control Huh7 cells and cholesterol-lipid (150 mg/l) treated Huh7 cells for indicated time points. β-Actin was used as loading control (upper panel). Lower panel shows plot of β-Actin normalized band intensity quantification of relative cellular Dicer1 levels upon indicated time of cholesterol-lipid treatment (n = 4 independent experiments; P = 0.0284, 0.0299).

(D, E) Dicer1 levels in Huh7 cells treated with BSA-Palmitate in a time dependent (D) and dose dependent manner (E). Western blot was done to measure the indicated protein levels. β-Actin was used as loading control (upper panels). Lower panels depict bar graph of β-Actin normalized band intensity quantification of relative cellular Dicer1 levels (n = 2 independent experiments).

(F, G) Cellular Dicer1 levels on exposure to lipids in mouse primary hepatocytes. Western blot was done to estimate the amount of cellular Dicer1 levels of mouse primary hepatocytes treated with increasing concentration of cholesterol-lipid concentrate (F) or BSA-Palmitate (G). β-Actin was taken as loading control. β-Actin normalized band intensity values of relative cellular Dicer1 are depicted below the respective lanes.

(H) Dicer1 levels in normal chow diet (ND) and Methionine Choline deficient (MCD) diet fed mice liver were measured by western blot detection from 50 µg total protein of mice liver lysates.

(I) Graph showing the relative levels of Dicer1 mRNA in control and cholesterol (150 mg/l for 4 hours) treated Huh7 cells. Quantification of Dicer1 mRNA was done by RT-qPCR analysis using gene specific primers from 200 ng of isolated RNA. Data was normalized with respect to GAPDH mRNA levels (n = 4 independent experiments; P = 0.1170).

(J) Effect of inhibition of proteasomal degradation on the cellular level of Dicer1 in cholesterol treated Huh7 cells. Western blot analysis showing the cellular level of Dicer1 in control and cholesterol (150 mg/l for 4 hours) treated Huh7 cells that were pre-treated with either ethanol or the proteasomal inhibitor MG132 (20 µM). MG132 treatment was done for 5 hours and cholesterol was added for the last 4 hours of MG132 treatment time. Total cellular protein ubiquitination was checked using anti-Ubiquitin antibody. β-actin was taken as loading control.

(K) Effect of the autophagy inhibitor Bafilomycin on the cellular Dicer1 levels in cholesterol treated Huh7 cells. Western blot showing Dicer1 levels in control and cholesterol (150 mg/l) challenged Huh7 cells that were pre-treated with either DMSO or Bafilomycin (100 nM). Bafilomycin treatment to Huh7 cells was done for 8 hours and cholesterol was added for the last 4 hours of Bafilomycin treatment time. Levels of LC3B were also analyzed by western blot. β-Actin was taken as loading control.

Data are represented as mean ± SD; ns: non-significant, *P < 0.05, **P < 0.01, ***P < 0.001, ****P<0.0001. For (2A), P-values were calculated using a one-way analysis of variance (one-way ANOVA) with Tukey post-hoc test. Otherwise, P-values were calculated by utilising two-tailed, paired Student's *t*-test.

Figure 3 Extracellular export of Dicer1 from lipid-treated hepatocytes

(A) Effect of GW4869 treatment on endogenous Dicer1 levels in control and cholesterol treated Huh7 cells. Western blot detection of Dicer1 in control and 150 mg/l cholesterol treated (4 hours) Huh7 cells that were pre-treated with either DMSO or GW4869. β-Actin was used as loading control.

(B) Cellular protein levels of exogenously expressed NH-Dicer1 inHuh7 cells treated with 150 mg/l of cholesterol-lipid concentrate for indicated time points. Western blot of cellular NH-Dicer1 levels in control and cholesterol-lipid treated Huh7 cells was done using anti-HA

antibody. β-Actin was used as loading control. β-Actin normalized band intensity values representing relative cellular NH-Dicer1 levels are indicated below the respective lanes.

(C, D) Nanoparticle tracking analysis of the EVs isolated from culture supernatant of control and lipid treated Huh7 cells. Representative graphs generated from Nanoparticle Tracking Analysis (NTA) depicting the size and concentration profile of isolated EVs from culture supernatant of control Huh7 (C, left panel), cholesterol (150 mg/l) treated Huh7 (C, right panel), fatty acid free BSA treated Huh7 (D, left panel) and BSA-Palmitate (0.5 mM) treated Huh7 (D, right panel) are shown.

(E) Data depicting the number of EVs released per cell as quantified by NTA of EVs isolated from culture supernatants of control versus cholesterol treated Huh7 cells (left panel, n = 4 independent experiments; $P < 0.0001$) and fatty acid free BSA versus BSA-Palmitate treated Huh7 cells (right panel, n = 4 independent experiments; $P < 0.0001$).

(F) Graphs showing the mean size of EVs as determined by NTA of EVs isolated from culture supernatants of control and cholesterol treated Huh7 cells (left panel, n = 4 independent experiments; $P = 0.0129$) as well as from fatty acid free BSA and BSA-Palmitate treated Huh7 cells (right panel, n = 4 independent experiments; $P = 0.0140$).

(G) Exogenously expressed NH-Dicer1 levels in extracellular vehicles (EVs) isolated from culture supernatant of Huh7 cells treated with 150 mg/l of cholesterol-lipid concentrate for indicated time points. Western blotting analysis was done with anti-HA antibody to detect the amount of NH-Dicer1. CD63 and Alix were used as markers for EVs. Cellular and EV associated levels of Calnexin and Flotillin-1 were also checked.

(H) Effect of BSA-Palmitate treatment on NH-Dicer1 content of EVs. EVs from culture supernatants of control (fatty-acid free BSA treated) and 0.5 mM BSA-Palmitate treated (16 hours) Huh7 cells were isolated, protein was extracted and western blot analysis of NH-Dicer1 was done using anti-HA antibody. CD63 was used as a marker for isolated EVs. Cellular and EV associated NH-Dicer1, Calnexin, ApoE and Flotillin1 were also western blotted.

(I) EV associated miR-122 levels from control and cholesterol treated Huh7 cells (left panel, n = 4 independent experiments; $P = 0.0015$) or fatty acid free BSA (BSA) and BSA-Palmitate treated Huh7 cells (right panel, n = 3 independent experiments; $P = 0.0134$). EVs were isolated from culture supernatant of Huh7 cells treated either with 150 mg/l of cholesterol or 0.5 mM of BSA-Palmitate, RNA was isolated and qRT-PCR quantification of miR-122 was done from 100

ng of isolated RNA. Data was normalized with respect to protein content of EVs isolated in each case.

(J) RNase protection assay of EV associated miR-122. EVs isolated from conditioned media of 150 mg/l cholesterol treated Huh7 cells were digested with RNase (100µg/ml) at 30^0C for 60 mins in presence or absence of Triton X-100. Post reaction, RNA was isolated followed by quantification of miR-122 by RT-qPCR. Ct values obtained were plotted n = 3 independent experiments; P = 0.3255, < 0.0001, < 0.0001).

(K) Quantification of circulating miRNAs in serum of MCD diet fed mice. Serum was isolated from normal chow diet and MCD diet fed mice. RT-qPCR detection of miRNAs was done from 100 ng of serum associated RNA (n = 2 for normal chow diet fed mice and n = 3 for MCD diet fed mice; P = 0.0106, 0.9105, 0.1235, 0.4361, respectively)

(L-M) Effect of Atorvastatin treatment on the cellular and EV associated abundance of Dicer1. Cellular Dicer1 and Ago2 levels of Huh7 cells cultured in serum free DMEM and treated with indicated concentration of Atorvastatin were detected by western blot analysis. β-Actin was used as loading control (L). Western blot analysis of EV associated NH-Dicer1 levels from Huh7 cells (cultured in serum free DMEM) treated with indicated concentration of Atorvastatin. CD63 was blotted as a marker of EV (M).

Data are represented as mean ± SD; ns: non-significant, *P < 0.05, **P < 0.01, ***P < 0.001, ****P<0.0001. P-values were calculated by utilising two-tailed, unpaired Student's *t*-test

Figure 4 Endosome maturation is required for Dicer1 export from lipid-challenged hepatocytes

(A-D) Effect of inhibition of endosomal maturation on Dicer1 levels in control and cholesterol-lipid (150 mg/l) treated Huh7 cells. Western blot analysis showing the cellular Dicer1 levels in control and 150 mg/l cholesterol-lipid treated Huh7 cells, depleted for Rab5A (A), HRS (B), Rab7A (C) or Alix (D). β-actin was used as loading control. Knockdown efficiency was also validated by western blot of the respective depleted factors. β-Actin normalized relative cellular Dicer1 levels were plotted for the respective blots in panel A and C (n = 3 for A; n = 2 for B and n = 4 for C).

(E) Effect of siAlix treatment on cellular miR-122 and Dicer1 levels in control and cholesterol-lipid (150 mg/l) treated Huh7 cells for 4 hours. Left panel shows the relative miR-122 cellular levels quantified by qRT-PCR detection from 25 ng of isolated cellular RNA Normalization was done against U6 snRNA (n = 3 independent experiments; P = 0.0044, 0.8497). Right

panel shows the band intensity quantification of relative cellular Dicer1 levels as quantified from western blot analysis of cellular Dicer1 levels. β-Actin was used as loading control for normalization (n = 4 independent experiments; paired *t* test, P = 0.0379, 0.8393).

(F) Effect of Alix knockdown on EV content of miR-122 and NH-Dicer1 from control and cholesterol-lipid (150 mg/l) treated Huh7 cells. EVs were isolated from culture supernatants of NH-Dicer1 expressing, siControl and siAlix transfected Huh7 cells treated with cholesterol-lipid (4 hours), RNA was isolated and miR-122 levels were measured by qRT-PCR from 100 ng of isolated RNA and normalized against the protein content of isolated EVs (upper left panel, n = 3 independent experiments, P = 0.0032, 0.0040). Western blot of EV associated NH-Dicer1 level is shown in lower left panel. CD63 was used as a marker of isolated EVs. Plot of relative EV associated NH-Dicer1 levels as obtained from band intensity quantification are shown in right panel. EV marker protein was used for normalization (n = 3 independent experiments).

(G, H) Graphs showing the mean size of EVs (G) [n = 4 independent experiments] and number of EVs released per cell (H) [n = 4 independent experiments, P = 0.0005, 0.3795, 0.0003, 0.3336) as obtained from Nanoparticle tracking (NTA) analysis of EVs isolated from culture supernatants of siControl and siAlix transfected Huh7 cells that were untreated or treated with cholesterol (150 mg/l) for 4 hours.

(I) EV content of different miRNAs (miR-16, miR-21, miR-24) from siControl and siAlix transfected Huh7 cells treated with or without cholesterol-lipid (150 mg/l) for 4 hours. RT-qPCR detection of miRNAs was done from 100 ng of isolated RNA from EV extracts and normalized against the protein content of EVs (n = 2 independent experiments; P = 0.0326 and 0.0330 for miR-16; P = 0.0012 and 0.0139 for miR-21; P = 0.0001 and 0.0001 for miR-24).

Data are represented as mean ± SD; ns: non-significant, *P < 0.05, **P < 0.01, ***P < 0.001, ****P<0.0001. P-values were calculated by utilising two-tailed, unpaired Student's *t*-test in most cases unless mentioned otherwise.

Figure 5. Redistribution of ER-endosome contacts causes loss of interaction between NH-Dicer1 and Ago2 in lipid treated Huh7 cells leading to impairment of Dicer1 processivity and miR-122 loading onto Ago2.

(A-B) Effect of lipid treatment on the interaction between NH-Dicer1 and Ago2 proteins in Huh7 cells transiently expressing NH-Dicer1. Western blot analysis of immunoprecipitated NH-Dicer1 (using anti-HA antibody) and its associated Ago2 protein levels in control Huh7 cells and in Huh7 cells treated with either 150 mg/l cholesterol-lipid for 4hours (A) or 0.5 mM

BSA-Palmitate for 16 hours (B). Input levels of the indicated proteins were western blotted. Quantification of western blot bands was done and band intensity ratio of Ago2 is to NH-Dicer1 indicating amount of Ago2 co-immunoprecipitated per unit NH-Dicer1 was calculated. The values were normalized against the respective control sets and shown below the blots.

(C) Interaction of transiently expressed FH-Ago2 with P-body protein Xrn1 and miR-122 in control and lipid treated Huh7 cells studied by immunoprecipitation assay. Western blot analysis showing pulled down FH-Ago2 (using anti-HA antibody) and its associated P-body factor, Xrn1 in control and BSA-Palmitate treated Huh7 cells transiently expressing FH-Ago2. Input levels of the proteins are also shown (left panel). Right panel shows the effect of cholesterol-lipid (150 mg/l) treatment on FH-Ago2 bound miR-122 in Huh7 cells transiently expressing FH-Ago2. Immunoprecipitation of FH-Ago2 (using anti-HA antibody) was done from control and cholesterol treated (for 4 h) Huh7 cell lysates. Immunoprecipitated samples were divided into two equal parts. Western blot was done with one part to quantify the amount of FH-Ago2 pulled down. RNA was isolated from the other part followed by quantification of miR-122 by qRT-PCR and normalization against the amount of FH-Ago2 pulled down (n = 3 independent experiments; P = 0.0223).

(D-E) Relative amount of miR-122, miR-122* and precursor miR-122 (pre-miR-122) bound to NH-Dicer1 that were immunoprecipitated (using anti-HA antibody) from control and cholesterol-lipid (150 mg/l) treated Huh7 cells expressing NH-Dicer1. Immunoprecipitated samples were divided into two equal parts. Western blot was done with one part to quantify the amount of NH-Dicer1 pulled down. miR-122, miR-122* (D) and pre-miR-122 (E) were quantified by qRT-PCR with the RNA isolated from immunoprecipitated materials and normalized to the amount of NH-Dicer1 immunoprecipitated(n = 3 independent experiments, P = 0.0233 and 0.0051 for miR-122 and miR-122* respectively; n = 5 independent experiments, P = 0.0245 for pre-miR-122).

(F) Western blot analysis of the amount of Ago2 co-immunoprecipitated with NH-Dicer1 in siControl and siAlix transfected, cholesterol treated Huh7 cells. Huh7 cells transiently expressing NH-Dicer1 were co-transfected with either siControl or siAlix followed by cholesterol-lipid (150 mg/l) treatment. The resulting cell lysates were immunoprecipitated with anti-HA antibody and western blotted for the indicated proteins. Input levels of NH-Dicer1, Ago2, Alix and β-Actin are also shown. Ratio of band intensity of Ago2 to immunoprecipitated NH-Dicer1 was calculated. The value was normalized against the siControl transfected and cholesterol treated set and shown below the blot.

(G-I) Subcellular distribution of NH-Dicer1 and miR-122 in Huh7 cells. Scheme of subcellular fractionation of Huh7 cells on a 3-30% OptiPrep™ (iodixanol) gradient (G). Huh7 cells transiently expressing NH-Dicer1 were treated with or without 150 mg/l cholesterol-lipid concentrate for 4 hours. Cells were lysed in isotonic buffer and post-nuclear supernatants were subject to ultracentrifugation on a 3-30% OptiPrep™ gradient for separation of subcellular organelles. After ultracentrifugation, ten fractions were collected by aspiration from top of the tube. Western blot analysis was done to detect the amount of NH-Dicer1 in each fraction (H). Calnexin and Alix were used as markers of endoplasmic reticulum (ER) and endosomes/multivesicular bodies (MVBs), respectively. Positions of the respective organelles are marked on top of the blots. Western blot of cellular NH-Dicer1 levels in control and cholesterol-lipid concentrate (150 mg/l) treated Huh7 cells are shown as input. Plot of Ct values of miR-122 in the MVB and ER fractions were obtained by qRT-PCR detection of RNA extracted from pooled fractions 2, 3, 4 (representing endosomes/MVBs) and pooled fractions 7, 8, 9 (representing ER) in control and cholesterol treated Huh7 cells (I, n = 3 independent experiments; P = 0.0001, 0.1083 for ER and endosomes/MVBs, respectively).

(J-K) Association of NH-Dicer1 with miR-122 and Ago2 in endosomes/multivesicular bodies upon cholesterol treatment. Huh7 cells transiently expressing NH-Dicer1 were treated with or without 150 mg/l cholesterol for 4 hours followed by lysis of cells under isotonic condition. Lysates were cleared and the post-nuclear supernatants were resolved on a 3-30% OptiPrep™ gradient for separation of subcellular organelles. Pooled fractions 2, 3, 4 (representing endosomes/MVBs) were immunoprecipitated for NH-Dicer1 (with anti-HA antibody). For detection of NH-Dicer1 bound miR-122, immunoprecipitated extracts were divided into two equal parts. From one part, levels of NH-Dicer1 pulled down were detected by western blot (J, lower panel). With the other part, amount of miR-122 associated with pulled-down NH-Dicer1 were quantified by qRT-PCR detection of miR-122 in RNA isolated from immunoprecipitated extracts and normalized against the amount of NH-Dicer1 immunoprecipitated (J, upper panel, n = 3 independent experiments; P = 0.0053). For detection of NH-Dicer1 bound Ago2 in endosomal/MVB fractions, western blot of immunoprecipitated NH-Dicer1 and associated Ago2 was done (K). Input levels of NH-Dicer1 and Ago2 in the endosome/MVB fractions was also western blotted (K).

(L) Representative images depicting the distribution of ER and endosomes in control Huh7 and 150 mg/l cholesterol-lipid treated (4 hours) Huh7 cells. Huh7 cells were co-transfected with plasmids encoding an ER localizing variant of dsRed (ER-dsRed) and endosome localizing variant of GFP (Endo-GFP). ER-ds Red and Endo-GFP signals were detected by direct immunofluorescence. Fields have been detected at 60x magnification. Scale bar

represents 10 μm. Rightmost column represents merged 3D surface reconstructions of ER and endosome, depicting their relative spatial distribution.

Data are represented as mean ± SD; ns: non-significant, *P < 0.05, **P < 0.01, ***P < 0.001, ****P<0.0001. P-values for (I) were calculated by utilising two-tailed, unpaired Student's *t*-test. Otherwise, P-values were calculated by utilising two-tailed, paired Student's *t*-test.

Figure 6. HuR-mediated Ago2-Dicer1 interaction loss causes export of Dicer1 from hepatocytes experiencing lipotoxic stress

(A) Western blot analysis of cellular levels of endogenous HuR protein in Huh7 cells treated with increasing concentration (0, 60, 150 mg/l) of cholesterol-lipid cholesterol for 4h. β-Actin was used as loading control. Quantification of β-Actin normalized relative cellular HuR levels was done and shown below the blots (n = 2 independent experiments).

(B) Cellular levels of Dicer1 protein estimated by western blot analysis from siControl and siHuR transfected Huh7 cells treated with or without cholesterol (150 mg/l) for 4h. β-Actin was used as loading control. Ratio of band intensities of Dicer1 is to β-Actin for each lane was calculated followed by normalisation against the untreated, siControl transfected set and was denoted below the blot. Downregulation of HuR was confirmed by western blot.

(C) Western blot analysis showing cellular levels of Dicer1 and Ago2 in Huh7 cells transfected with increasing amount of HA-HuR (200,400,1000ng per well for a 12 well cell culture). pCIneo was transfected in Huh7 cells as control. Expression levels of HA-HuR were confirmed by western blot using anti-HA antibody. β-Actin was used as loading control (left panel). β-Actin normalized relative cellular Dicer1 levels were quantified and plotted (right panel) [n = 2 independent experiments].

(D) Effect of HA-HuR expression on EV content of NH-Dicer1. EVs were isolated from culture supernatant of Huh7 cells either expressing pCIneo or HA-HuR. Western blot analysis of EV associated NH-Dicer1 was done from the EV protein extract. Alix was used as an EV marker protein.

(E) Effect of HA-HuR expression on the interaction between Ago2 and Dicer1 in Huh7 cells. Endogenous Dicer1 was immunoprecipitated from control and HA-HuR expressing Huh7 cell extracts. Western blot analysis shows the amount of Ago2 that co-immunoprecipitated with Dicer1 protein. Also shown are the input levels of Dicer1, Ago2, HA-HuR and β-Actin. pCIneo was transfected in control Huh7 cells. HC stands for heavy chain.

(F, G) Consequence of ectopic expression of various HuR mutants on cellular Dicer1 level in Huh7 cells. Huh7 cells were transfected with plasmids encoding either Myc-tagged full length HuR (Myc-HuR-FL) or Myc-tagged deletion mutants of HuR, namely Myc-HuR ΔI, Myc-HuR ΔII, Myc-HuR ΔIII, Myc-HuR ΔB. pCIneo was transfected as control. A schematic depiction of the HuR constructs is shown in (F). Western blot analysis of cellular Dicer1 and expression levels of the Myc-tagged HuR proteins were done. β-Actin was probed as loading control (G).

(H) Effect of ectopic expression of FH-Ago2 (200 and 400 ng for 0.5 x 10^6 cells) or pCIneo-GFP (400 ng for 0.5 x 10^6 cells) on endogenous Dicer1 level in Huh7 cells untreated or treated with 150 mg/l cholesterol-lipid concentrate for 4h. Relative levels of Dicer1 have been calculated from band intensities and normalized against β-Actin followed by further normalization against the respective untreated set. The values are denoted below the respective lanes.

(I) Cellular Dicer1 levels in HA-HuR expressing Huh7 cells that were co-transfected with FH-Ago2. Huh7 cells were transfected with either HA-HuR only or co-transfected with HA-HuR and FH-Ago2. pCIneo was transfected as control. Western blot analysis of cellular Dicer1 level was done. Expression of HA-HuR and FH-Ago2 was also confirmed by western blot. β-Actin was taken as loading control.

Figure7. Exocytosis of Dicer1 counters ER stress in high lipid exposed hepatic cells.

(A) Alterations in lipid metabolic genes induced upon treatment with cholesterol-lipid concentrate (150 mg/l) for 4 hours. RT-qPCR detection of mRNAs using gene specific primers was done from 200ng of total cellular RNA Normalization was done using β-Actin mRNA (n = 6 independent experiments, P = 0.0018 for LDLR; n = 6 independent experiments, P = 0.0033 for HMGCR; n = 6 independent experiments, P <0.0001 for ACAT2; n = 6 independent experiments, P = 0.4681 for CPT1A; n = 5 independent experiments, P = 0.0015 for SCD; n = 3 independent experiments; P = 0.0143 for CYP7A1; n = 4 independent experiments, P = 0.1418 for SOAT1). Abbreviations: LDLR; Low Density Lipoprotein Receptor, HMGCR; 3-Hydroxy 3-Methylglutary-CoA Reductase, ACAT2; Acetyl Co-A acetyltransferase 2, CPT1A; Carnitine palmitoyl transferase 1A, SCD; Stearoyl Co-A Desaturase, CYP7A1; Cholesterol 7 alpha-hydroxylase, SOAT1; Sterol-O-Acyltransferase 1.

(B) Ectopic expression of NH-Dicer1 in lipid treated cells leads to amplified expression of deregulated lipid metabolic genes. Huh7 cells treated with cholesterol-lipid concentrate (150 mg/l) were transfected with (1µg/ 1 x 10^6 cells) plasmid encoding either NH-Dicer1 or control vector (pCI-Neo). RT-qPCR detection of mRNAs using gene specific primers was done from 200 ng of total cellular RNA. Normalization was done using β-Actin mRNA (n ≥ 3 independent experiments, P = 0.1501 for LDLR; n ≥ 3 independent experiments, P = 0.2381 for HMGCR; n = 4 independent experiments, P = 0.0588 for ACAT2; n = 4 independent experiments, P = 0.1585 for CPT1A; n = 4 independent experiments, P = 0.0535 for SCD; n = 4 independent experiments, P = 0.3194 for SOAT1).

(C) Bodipy 493/503 staining of lipid droplets (LDs) in Huh7 cells treated with either 150 mg/l cholesterol (4h) or 0.5 mM BSA-Palmitate (16h) or control cells (only BSA). Cells were counterstained with DAPI to visualize the nucleus. Fields represent one of 6 fields detected at 60x magnification. Scale bar represents 10µm.

(D-E) ER stress and apoptosis is induced in cholesterol and palmitate treated Huh7 cells. Time dependent changes in eIF-2α, Phospho eIF2α (ER stress marker), and cleaved PARP (apoptosis marker) were detected by western blot analysisof cholesterol-lipid concentrate (150 mg/l) treated Huh7 cells. β-Actin was used as loading control (D). Indication of ER stress was measured by western blot analysis of cellular levels of P-eIF2α and eIF2α from Huh7 cells treated with indicated concentrations of BSA-Palmitate (16 hours). For control Huh7 cells, equivalent amount of fatty acid free BSA was added. β-Actin was used as loading control (E).

(F) Effect of thapsigargin treatment on cellular Dicer1 levels in Huh7 cells. Dicer1 levels were detected by western blot analysis of cell extracts from control and indicated concentrations of thapsigargin treated Huh7 cells. Phopsho-eIF2α levels were also western blotted as ER stress marker. β-actin was used as loading control.

(G) Effect of thapsigargin treatment on lipid droplet abundance in Huh7 cells. Representative bright field and fluorescence images showing lipid droplets stained with Bodipy 493/503 in control and 2.5μM thapsigargin treated Huh7 cells.

(H) NH-Dicer1 expression in lipid treated cells leads to elevated levels of the ER stress marker-Phospho-eIF2α and apoptosis marker- cleaved PARP. Huh7 cells transfected with NH-Dicer1 expressing plasmid (1μg/ 1 x 10^6 cells) or a control vector (pCINeo) were treated with 150 mg/l cholesterol-lipid concentrate for the indicated time points. Western blot detection of respective proteins using specific antibodies was done. β-Actin was used as the loading control.

(I-J) NH-Dicer1 expression in lipid treated cells lead to increased numbers of TUNEL positive nuclei. Huh7 cells were transfected with NH-Dicer1 expressing plasmid (1μg/ 1 x 10^6 cells) prior to cholesterol (150 mg/l) treatment for indicated time points. Cells expressing HA-tagged Dicer1 were detected by immunofluorescence using anti-HA primary antibodies and Alexa-488 labelled secondary antibodies (green). TUNEL staining was done and the percentage of TUNEL positive cells (red) were identified for cells that are expressing or not expressing HA-Dicer1 (I). White arrows indicate HA-positive cells showing TUNEL-positive nuclei. Scale bar indicates 100μm. (J) Graphical representation of the described experiment (n = 6 fields from 3 independent experiments; P = 0.1204, 0.0303, 0.0038).

(K) Elevated levels of cleaved PARP in NH-Dicer1 expressing cholesterol treated Huh7 cells could be reversed by anti-miR-122. Huh7 cells transiently expressing NH-Dicer1 were transfected with either 30 nM concentration of anti-miR-122 or anti-miR-21 or anti-miR negative control followed by cholesterol treatment (150 mg/l) for 8 hours. Western blot analysis of the cell lysates for NH-Dicer1, cleaved PARP and phospho-eIF2α were done. β-Actin was used as the loading control.

Data are represented as mean ± SD; ns: non-significant, *P < 0.05, **P < 0.01, ***P < 0.001, ****P<0.0001. P-values were calculated by utilising two-tailed, unpaired Student's *t*-test.

Figure 8 Dicer1 restoration in MCD-diet fed mice liver aggravates lipid accumulation, cellular stress and inflammation

(A) Schematic representation of the experiment. 8-10 weeks old male C57BL/6 mice were randomly divided into three groups. One group was fed a normal chow diet (ND) for 4 weeks. The second group was fed a Methionine Choline deficient diet (MCD) for 4 weeks with tail vein injection of 30 µg of control pCIneo plasmid administered on the 10^{th}, 18^{th} and 24^{th} day. The third group was also fed a Methionine Choline deficient diet (MCD) for 4 weeks along with tail vein injection of 30 µg of NH-Dicer1 expression plasmid was given on the 10^{th}, 18^{th} and 24^{th} day of the feeding period.

(B) Changes in the level of miR-122, pre-miR-122 and miR-21 in mouse liver. Quantification of relative levels of miR-122 (left panel, n = 4 number of mice per group; P <0.0001, 0.0740), pre-miR-122 (middle panel, n = 4 number of mice per group; P = 0.0103, 0.6781, Unpaired *t* test between MCD diet and MCD diet (+NH-Dicer1) group, P = 0.0068) and miR-21 (right panel, n = 3 number of mice per group; P = 0.0697) in mice liver was done by qRT-PCR detection from total liver RNA. miR-122 and miR-21 levels were quantified from 100 ng of liver tissue RNA and normalized with respect to U6 snRNA. pre-miR-122 was quantified from 200 ng of liver tissue RNA and normalized against GAPDH mRNA levels.

(C) Changes in mouse liver CAT-1 mRNA levels and serum miR-122 levels. Left panel shows the relative levels of CAT-1 mRNA as quantified by qRT-PCR detection from 200 ng of isolated liver RNA. GAPDH mRNA levels was quantified for normalization (n = 3 number of mice per group; P = 0.0313). Right panel shows the plot of Ct values as obtained from qRT-PCR detection of miR-122 from 50 ng of serum RNA (n = 3 number of mice per group; Unpaired *t* test, P = 0.0472, <0.0001, 0.0004).

(D) Western blot analysis of mouse liver lysate for the indicated proteins was done. Expression of NH-Dicer1 was checked in the liver lysates of mice. Endogenous levels of phospho-eIF2α, phospho-4EBP1, HuR and Ago2 were also measured by western blot analysis. β-Actin was used as loading control in all cases. Western blot was done from 15 µg of protein for each sample.

(E-G) Histological analysis of mouse liver sections. Hematoxylin and eosin-stained micrographs of normal chow diet (control diet) fed, MCD diet fed (pCIneo injected) and MCD diet fed (NH-Dicer1 injected) mouse liver sections of 5 µm thickness are shown. For each sample, images of both 10X and 20X magnification are shown. Scale bar represents 100 µm (E). Quantification of number of fat globules per field (F, Unpaired *t* test, P = 0.0010, <0.0001,

<0.0001) and hepatic fat globule diameter (G, Unpaired *t* test, P <0.0001, <0.0001, <0.0001) were done from micrographs of hematoxylin and eosin-stained liver sections and plotted (n = 4 fields for control diet; n = 8 fields for MCD diet (pCIneo injected); n = 8 fields for MCD diet (NH-Dicer1 injected).

(H) Expression profile of pro-inflammatory cytokine mRNA levels in mouse liver. Quantification of mRNA levels of IL-1β (left panel, n = 5 number of mice per group; P = 0.0500, 0.0363, Unpaired *t* test between MCD diet and MCD diet (+NH-Dicer1) group, P = 0.1690) and TNF-α (right panel, n = 5 number of mice per group; P = 0.0071, 0.0021, Unpaired *t* test between MCD diet and MCD diet (+NH-Dicer1) group, P = 0.0026) in mice liver was done from 200 ng of isolated liver RNA. Normalization was done with respect to GAPDH mRNA levels.

All data were generated from at least three different mice from each group. Data are represented as mean ± SD; ns: non-significant, *P < 0.05, **P < 0.01, ***P < 0.001, ****P<0.0001. P-values were calculated by utilising two-tailed, paired Student's *t*-test in most cases unless mentioned otherwise.

Figure 9 A schematic representation of the possible mechanism of Dicer1 and miR-122 export from lipid loaded hepatic cells. Under normal condition, miRNP nucleation occurs on the ER membrane followed by target mRNA repression. Repressed mRNA-miRNP complex then translocate to the endosomes from where miRNPs along with Dicer1 are recycled back for a fresh round of repression (16). However, in lipid exposed hepatic cells, differential compartmentalization of Ago2 and Dicer1 causes loss of Ago2-Dicer1 interaction. As a result, Dicer1 and miR-122 get exported out by the process that require endosomal maturation. HuR by favouring miRNA-uncoupling from Ago2 favours the Dicer1-Ago2 interaction loss to promote the export of miRNA from lipid-challenged hepatic cells (17). .

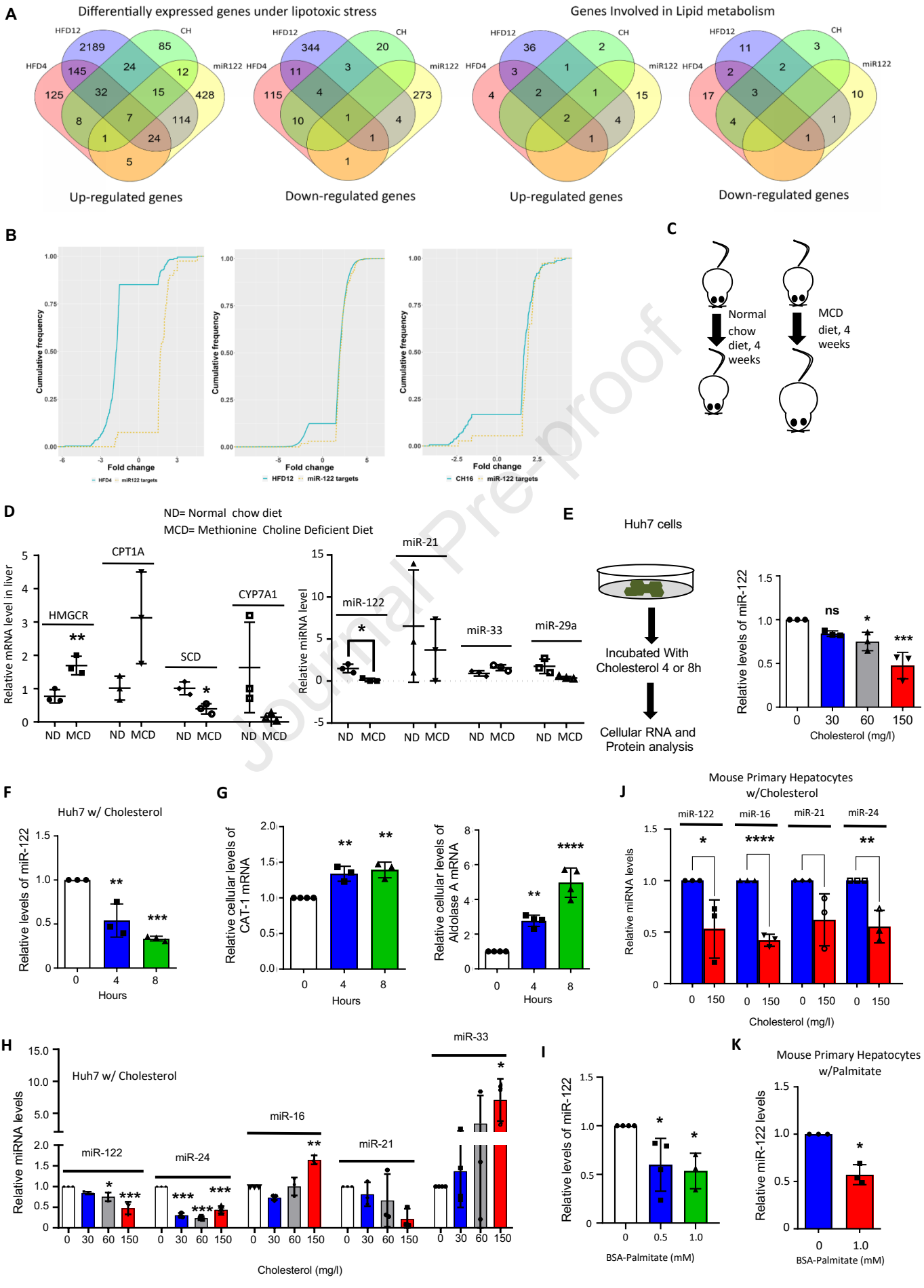
A
Differentially expressed genes under lipotoxic stress
Genes Involved in Lipid metabolism
HFD12
CH
HFD4
miR122
Up-regulated genes
Down-regulated genes
B
Cumulative frequency
Fold change
HFD4
miR122 targets
HFD12
miR-122 targets
CH16
C
Normal chow diet, 4 weeks
MCD diet, 4 weeks
D
ND= Normal chow diet
MCD= Methionine Choline Deficient Diet
Relative mRNA level in liver
HMGCR
CPT1A
SCD
CYP7A1
Relative miRNA level
miR-122
miR-21
miR-33
miR-29a
ND
MCD
E
Huh7 cells
Incubated With Cholesterol 4 or 8h
Cellular RNA and Protein analysis
Relative levels of miR-122
Cholesterol (mg/l)
F
Huh7 w/ Cholesterol
Hours
G
Relative cellular levels of CAT-1 mRNA
Relative cellular levels of Aldolase A mRNA
J
Mouse Primary Hepatocytes w/Cholesterol
miR-16
miR-24
Relative miRNA levels
H
Huh7 w/ Cholesterol
I
BSA-Palmitate (mM)
K
Mouse Primary Hepatocytes w/Palmitate
Relative miR-122 levels

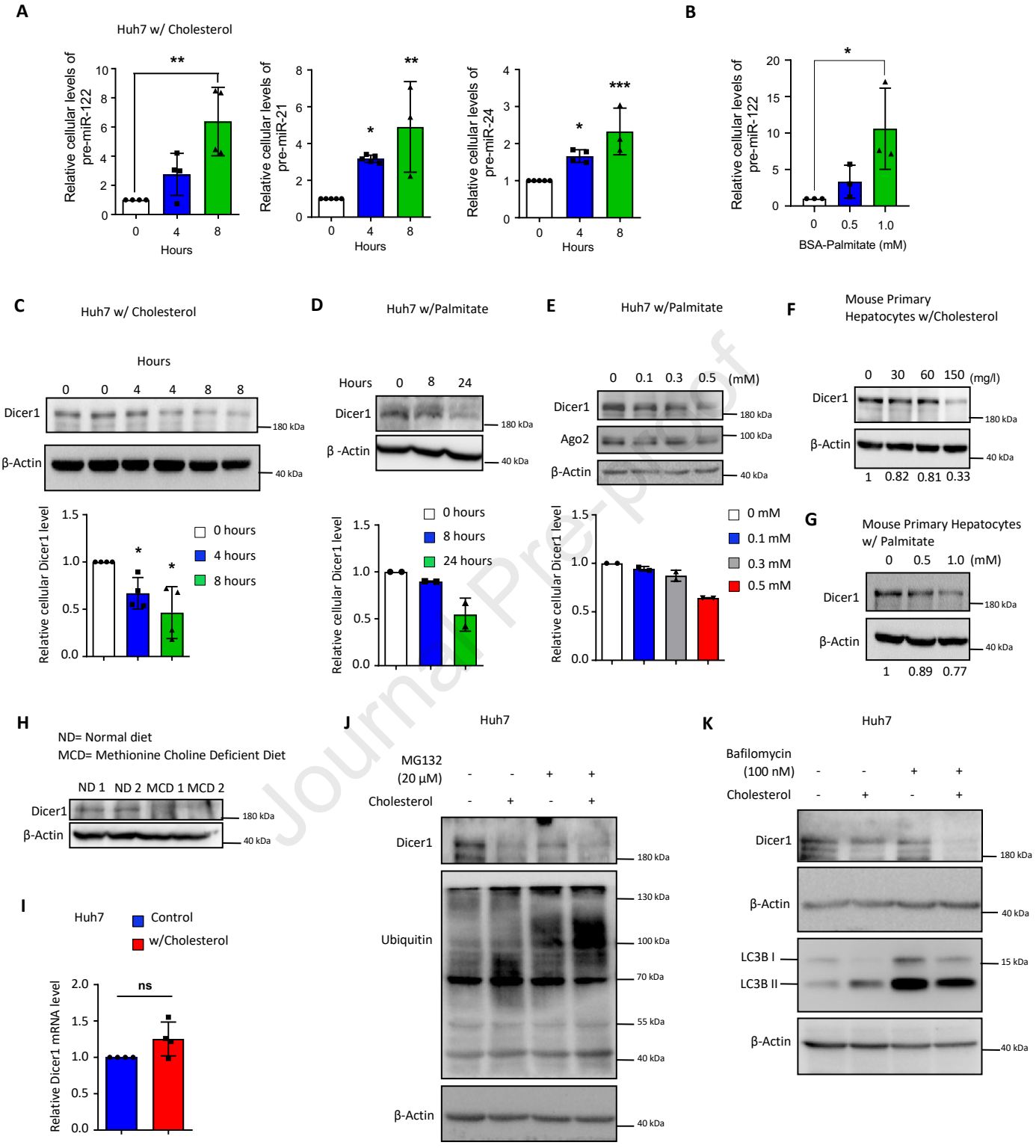

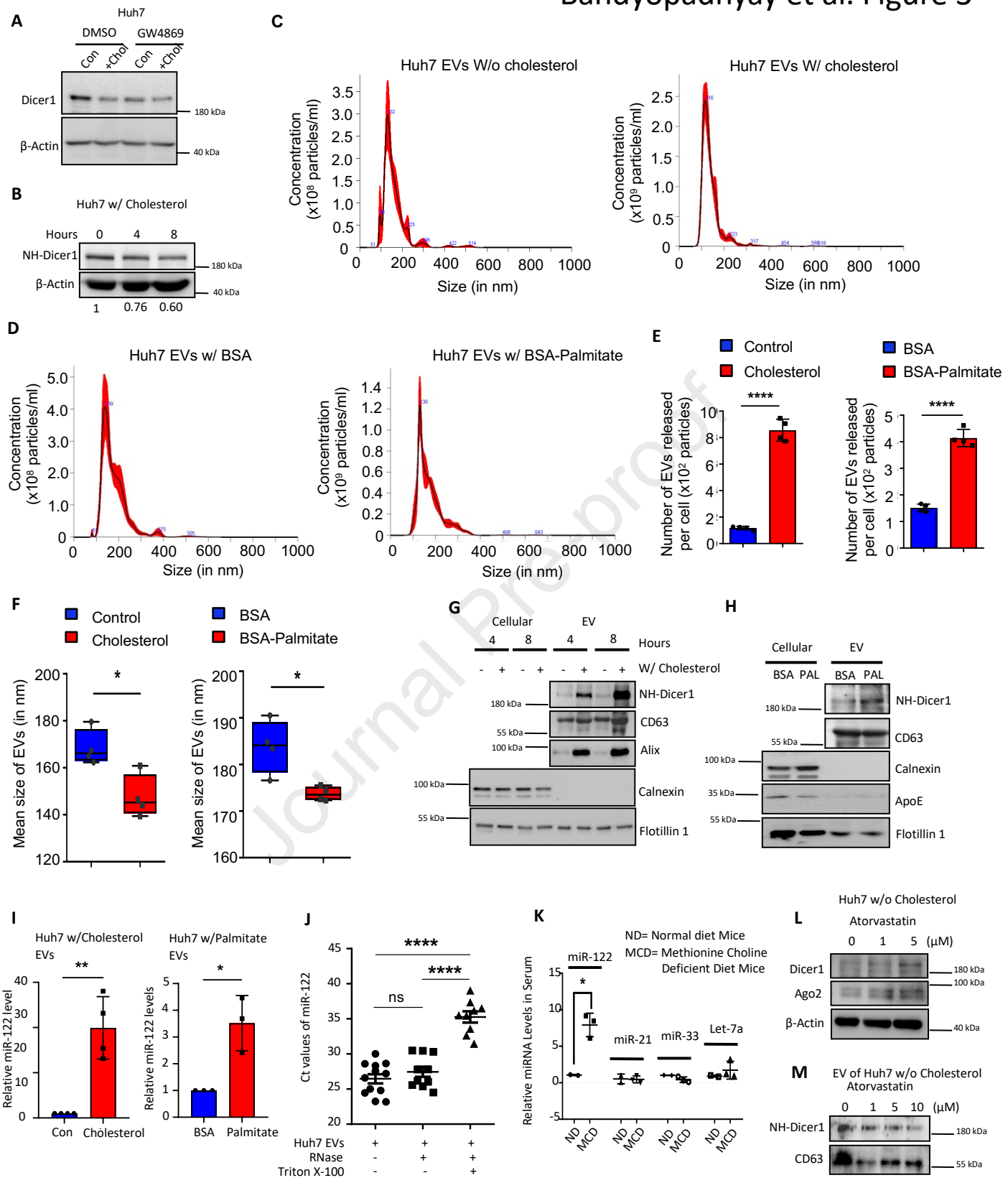

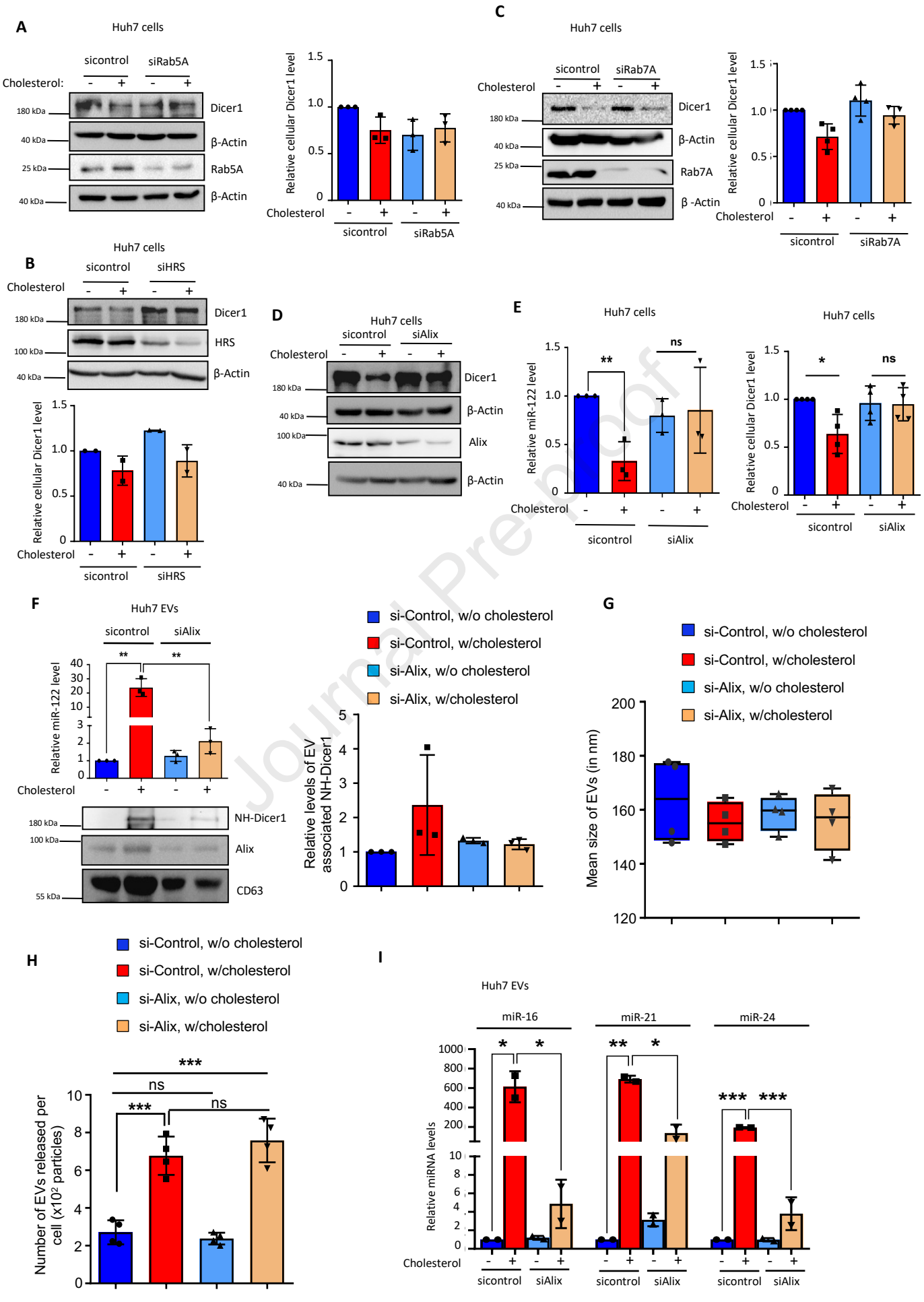
A
Huh7 cells
sicontrol
siRab5A
Cholesterol:
Dicer1
β-Actin
Rab5A
Relative cellular Dicer1 level
B
Huh7 cells
siHRS
HRS
C
Huh7 cells
siRab7A
Rab7A
D
Huh7 cells
siAlix
Alix
E
Huh7 cells
Relative miR-122 level
ns
F
Huh7 EVs
NH-Dicer1
CD63
Relative levels of EV associated NH-Dicer1
si-Control, w/o cholesterol
si-Control, w/cholesterol
si-Alix, w/o cholesterol
si-Alix, w/cholesterol
G
Mean size of EVs (in nm)
H
Number of EVs released per cell (x10² particles)
I
miR-16
miR-21
miR-24
Relative miRNA levels

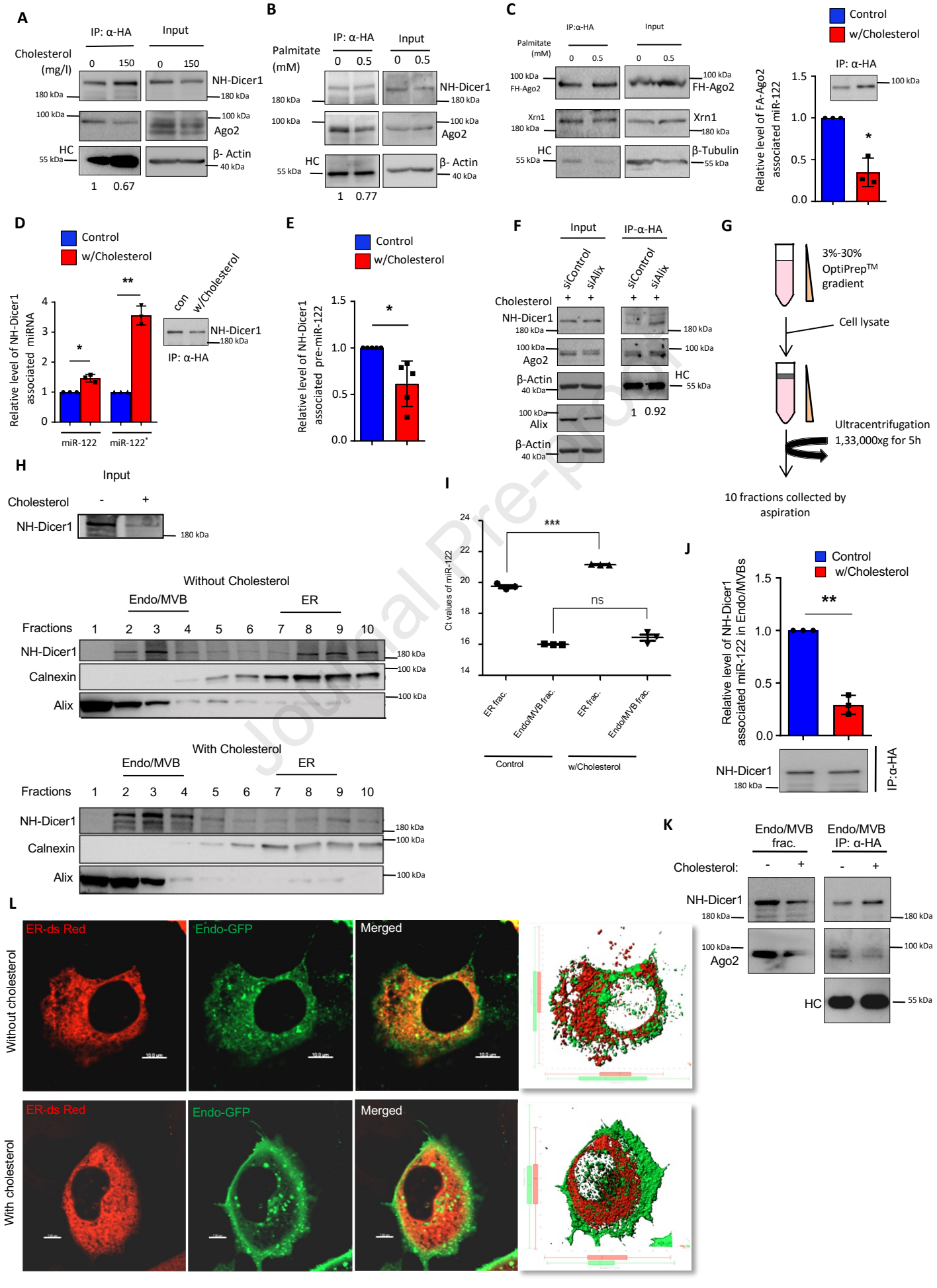
A
IP: α-HA
Input
Cholesterol (mg/l)
0
150
0
150
NH-Dicer1
180 kDa
Ago2
100 kDa
HC
55 kDa
β- Actin
40 kDa
1
0.67
B
IP: α-HA
Input
Palmitate (mM)
0
0.5
0
0.5
NH-Dicer1
180 kDa
Ago2
100 kDa
HC
55 kDa
β- Actin
40 kDa
1
0.77
C
IP:α-HA
Input
Palmitate (mM)
0
0.5
0
0.5
100 kDa
FH-Ago2
Xrn1
180 kDa
HC
55 kDa
β-Tubulin
55 kDa
Control
w/Cholesterol
IP: α-HA
Relative level of FA-Ago2 associated miR-122
100 kDa
D
Control
w/Cholesterol
Relative level of NH-Dicer1 associated miRNA
miR-122
miR-122*
con
w/Cholesterol
NH-Dicer1
180 kDa
IP: α-HA
E
Control
w/Cholesterol
Relative level of NH-Dicer1 associated pre-miR-122
F
Input
IP-α-HA
siControl
siAlix
Cholesterol
NH-Dicer1
180 kDa
Ago2
100 kDa
β-Actin
40 kDa
HC
55 kDa
Alix
1
0.92
G
3%-30% OptiPrep™ gradient
Cell lysate
Ultracentrifugation 1,33,000xg for 5h
10 fractions collected by aspiration
H
Input
Cholesterol
-
+
NH-Dicer1
180 kDa
Without Cholesterol
Endo/MVB
ER
Fractions
1
2
3
4
5
6
7
8
9
10
NH-Dicer1
Calnexin
Alix
180 kDa
100 kDa
With Cholesterol
I
Ct values of miR-122
***
ns
ER frac.
Endo/MVB frac.
Control
w/Cholesterol
J
Control
w/Cholesterol
Relative level of NH-Dicer1 associated miR-122 in Endo/MVBs
**
NH-Dicer1
180 kDa
IP:α-HA
K
Endo/MVB frac.
Endo/MVB IP: α-HA
Cholesterol:
NH-Dicer1
180 kDa
Ago2
100 kDa
HC
55 kDa
L
Without cholesterol
With cholesterol
ER-ds Red
Endo-GFP
Merged

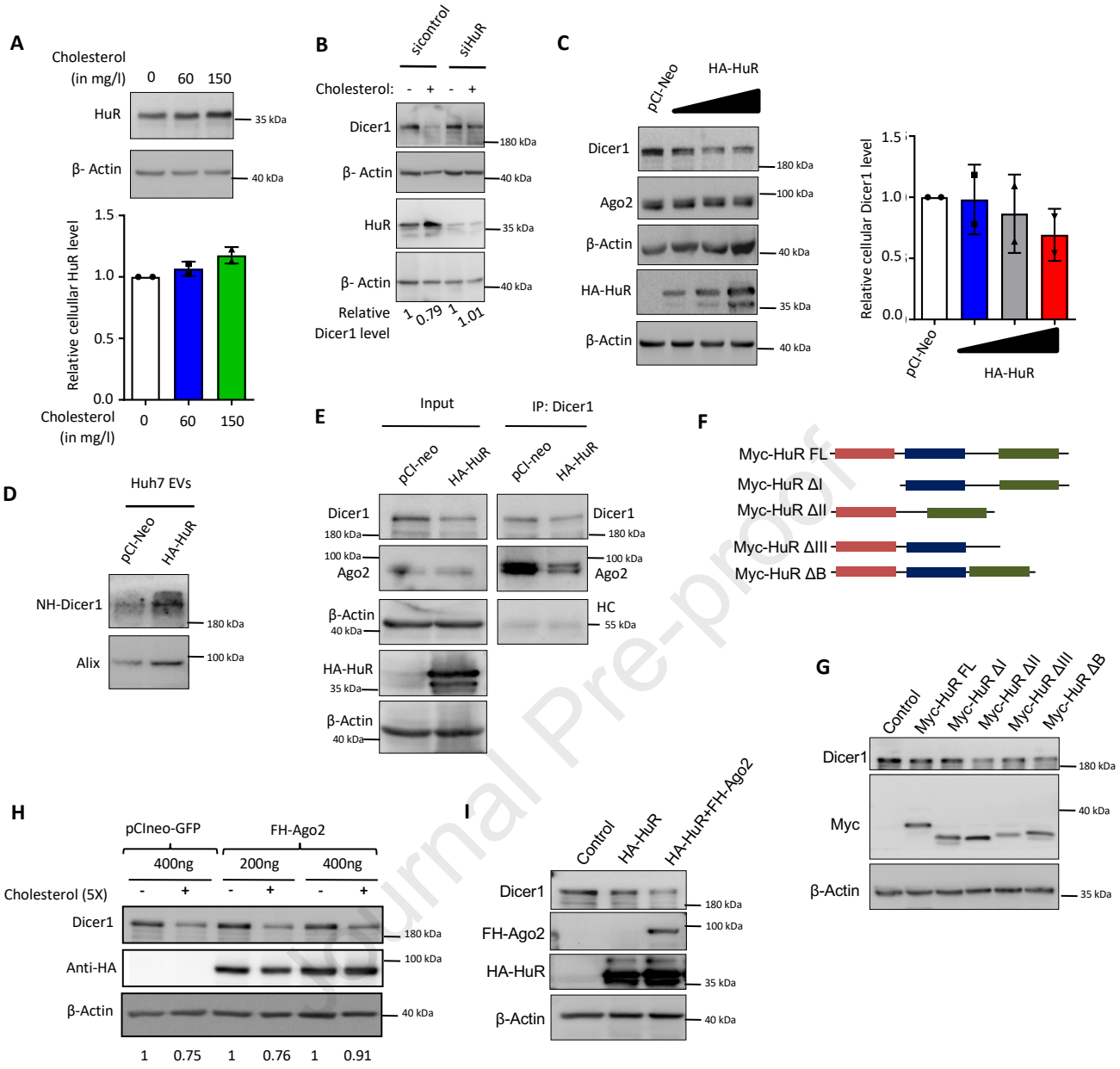
A
Cholesterol (in mg/l)
0
60
150
HuR
35 kDa
β- Actin
40 kDa
Relative cellular HuR level
1.5
1.0
0.5
0.0
B
sicontrol
siHuR
Cholesterol:
Dicer1
180 kDa
β- Actin
40 kDa
HuR
35 kDa
Relative Dicer1 level
1
0.79
1
1.01
C
pCI-Neo
HA-HuR
Dicer1
180 kDa
Ago2
100 kDa
β-Actin
40 kDa
HA-HuR
35 kDa
Relative cellular Dicer1 level
D
Huh7 EVs
pCI-Neo
HA-HuR
NH-Dicer1
180 kDa
Alix
100 kDa
E
Input
IP: Dicer1
pCI-neo
HA-HuR
Dicer1
Ago2
β-Actin
HA-HuR
HC
55 kDa
F
Myc-HuR FL
Myc-HuR ΔI
Myc-HuR ΔII
Myc-HuR ΔIII
Myc-HuR ΔB
G
Control
Myc-HuR FL
Myc-HuR ΔI
Myc-HuR ΔII
Myc-HuR ΔIII
Myc-HuR ΔB
Dicer1
Myc
β-Actin
H
pCIneo-GFP
FH-Ago2
400ng
200ng
400ng
Cholesterol (5X)
Dicer1
Anti-HA
β-Actin
1
0.75
1
0.76
1
0.91
I
Control
HA-HuR
HA-HuR+FH-Ago2
Dicer1
FH-Ago2
HA-HuR
β-Actin

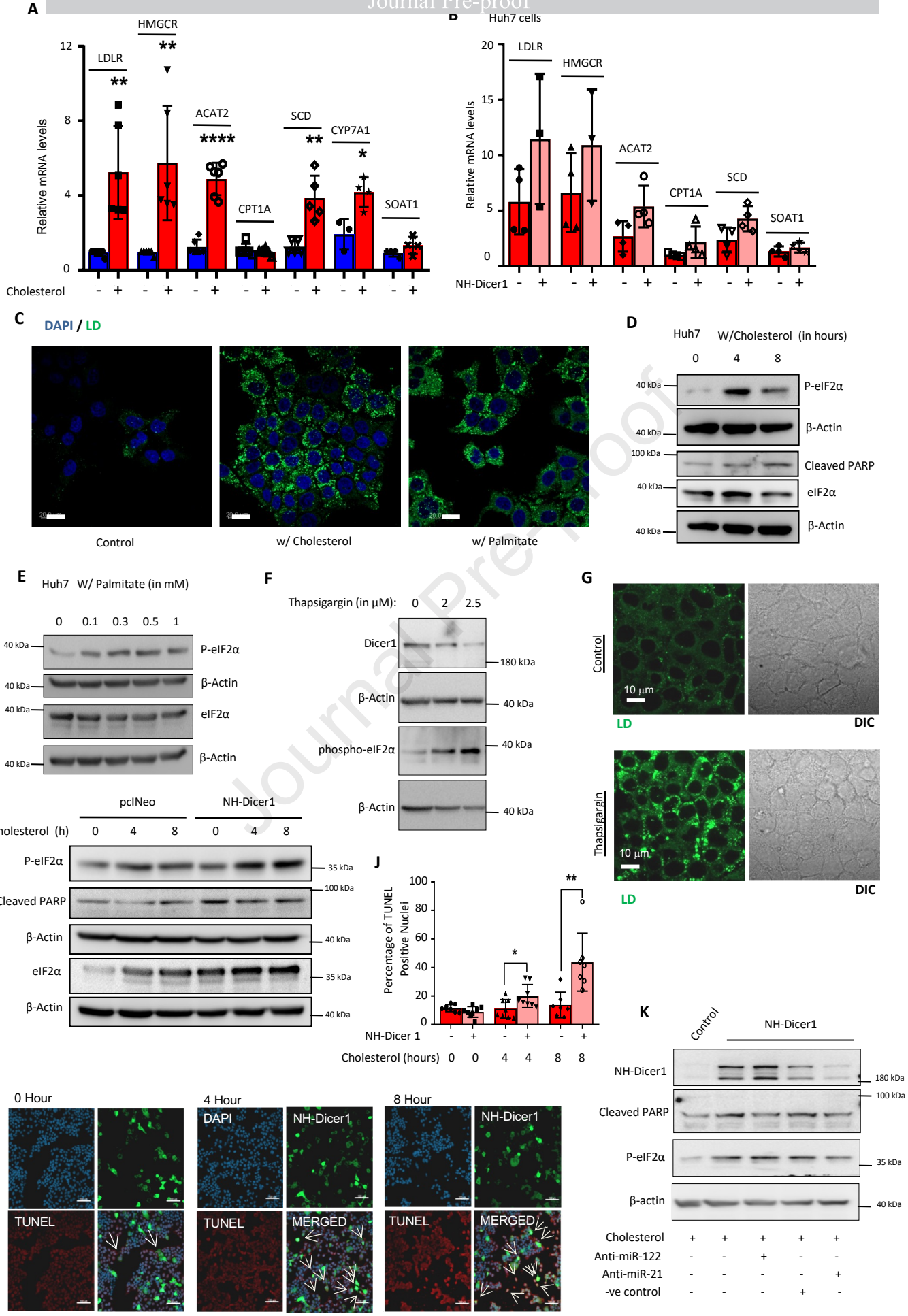
A
HMGCR
LDLR
ACAT2
SCD
CYP7A1
CPT1A
SOAT1
Relative mRNA levels
Cholesterol
B
Huh7 cells
LDLR
HMGCR
ACAT2
CPT1A
SCD
SOAT1
Relative mRNA levels
NH-Dicer1
C
DAPI / LD
Control
w/ Cholesterol
w/ Palmitate
D
Huh7 W/Cholesterol (in hours)
0 4 8
P-eIF2α
β-Actin
Cleaved PARP
eIF2α
β-Actin
E
Huh7 W/ Palmitate (in mM)
0 0.1 0.3 0.5 1
P-eIF2α
β-Actin
eIF2α
β-Actin
F
Thapsigargin (in μM): 0 2 2.5
Dicer1
β-Actin
phospho-eIF2α
β-Actin
G
Control
Thapsigargin
10 μm
LD
DIC
H
pcINeo
NH-Dicer1
Cholesterol (h) 0 4 8 0 4 8
P-eIF2α
Cleaved PARP
β-Actin
eIF2α
β-Actin
J
Percentage of TUNEL Positive Nuclei
NH-Dicer 1
Cholesterol (hours) 0 0 4 4 8 8
I
0 Hour
4 Hour
8 Hour
DAPI
NH-Dicer1
TUNEL
MERGED
K
Control
NH-Dicer1
NH-Dicer1
Cleaved PARP
P-eIF2α
β-actin
Cholesterol
Anti-miR-122
Anti-miR-21
-ve control

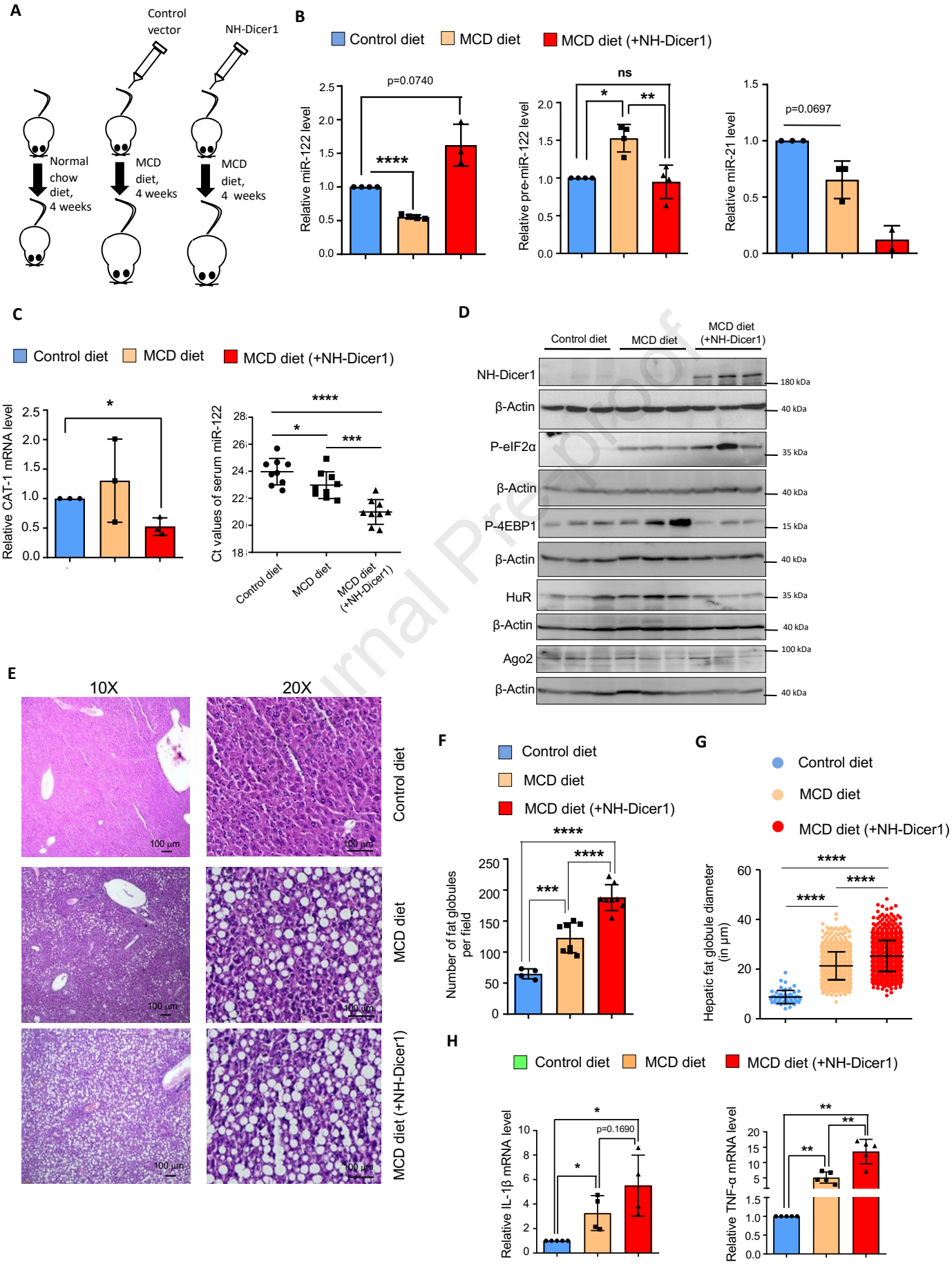
A
Control vector
NH-Dicer1
Normal chow diet, 4 weeks
MCD diet, 4 weeks
MCD diet, 4 weeks
B
Control diet
MCD diet
MCD diet (+NH-Dicer1)
Relative miR-122 level
p=0.0740
****
Relative pre-miR-122 level
ns
*
**
Relative miR-21 level
p=0.0697
C
Relative CAT-1 mRNA level
Ct values of serum miR-122
D
NH-Dicer1
β-Actin
P-eIF2α
P-4EBP1
HuR
Ago2
180 kDa
40 kDa
35 kDa
15 kDa
100 kDa
E
10X
20X
100 μm
F
Number of fat globules per field
G
Hepatic fat globule diameter (in μm)
H
Relative IL-1β mRNA level
p=0.1690
Relative TNF-α mRNA level

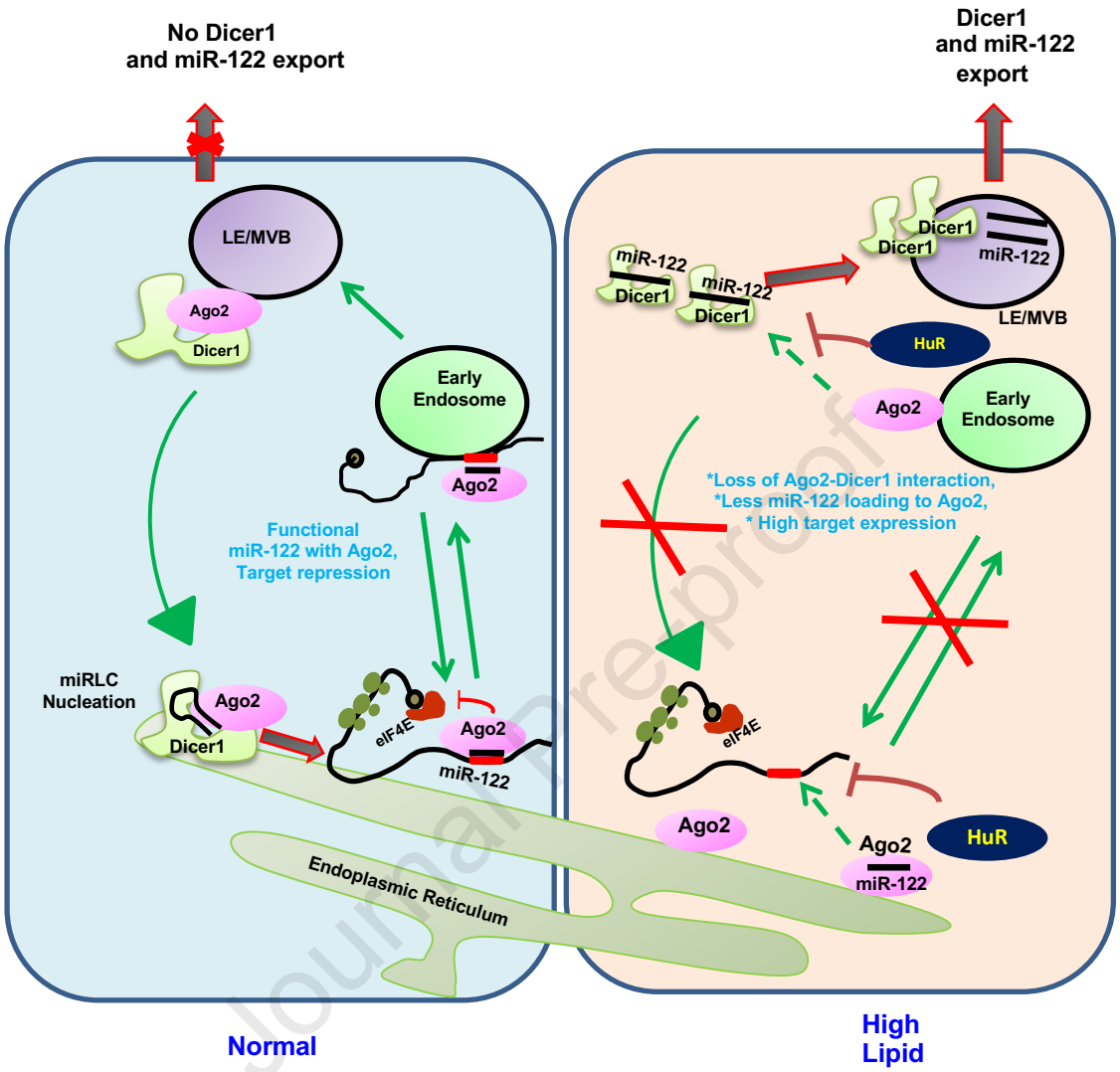

CRediT author statement

Diptankar Bandopadhyay: Writing- Original draft preparation, Methodology, Data generation and curation. : **Sudarshana Basu:** Writing- Original draft preparation, Methodology, Data generation and curation. : **Ishita Mukherjee.**: Software, Data generation and curation. :**Saikat Chakrabarti:** Supervision.**:Partha Chakrabarti:** Supervision.: **Kamalika Mukherjee:** Conceptualization and Editing, Writing.: **Suvendra Bhattacharyya**: Supervision, Conceptualization and Editing, Writing- Reviewing.